SIAM J. SCI. COMPUT.
Vol. 44, No. 4, pp. B1148–B1174

ROBUST MONOLITHIC SOLVERS FOR THE STOKES–DARCY PROBLEM WITH THE DARCY EQUATION IN PRIMAL FORM*

WIETSE M. BOON†, TIMO KOCH‡, MIROSLAV KUCHTA§, AND KENT-ANDRÉ MARDAL¶

Abstract. We construct mesh-independent and parameter-robust monolithic solvers for the coupled primal Stokes–Darcy problem. Three different formulations and their discretizations in terms of conforming and nonconforming finite element methods and finite volume methods are considered. In each case, robust preconditioners are derived using a unified theoretical framework. In particular, the suggested preconditioners utilize operators in fractional Sobolev spaces. Numerical experiments demonstrate the parameter-robustness of the proposed solvers.

Key words. Stokes–Darcy, preconditioning, parameter-robust solvers

MSC code. 65F08

DOI. 10.1137/21M1452974

1. Introduction.

In this work, we propose efficient solvers for multiphysics systems where a moving fluid (e.g., channel flow) governed by the Stokes equations in one subdomain interacts with fluid flow in porous media described by the Darcy equation in a neighboring subdomain. The main contribution is a framework which allows us to construct parameter-robust preconditioners for iterative solvers of linear systems arising from different discretizations of the coupled Stokes–Darcy problem. The theory is confirmed and complemented by extensive numerical experiments building on modern and open-source numerical software frameworks.

Systems exhibiting free flow coupled with porous medium flow are ubiquitous in nature, appearing in numerous environmental, industrial (see, e.g., [28] and references therein), and medical applications [62] . Discretization of the Stokes–Darcy problem is challenging with many finite element (e.g., [27, 38, 50, 44, 60, 61, 36, 19, 4]) and finite volume (e.g., [66, 65]) schemes devised with the aim to obtain robust approximation properties. Moreover, the coupled system presents a difficulty for construction of numerical solvers as in the applications the problem parameters weighting different terms of the equations may differ by several orders of magnitude due to, for example, variations in material parameters or large contrast of length scales (e.g., micro/macro-circulation modelling [46, 67]).

These challenges have been addressed in a number of works. In general, we can distinguish between monolithic approaches (where all the problem unknowns are

*Submitted to the journal's Computational Methods in Science and Engineering section October 15, 2021; accepted for publication (in revised form) May 17, 2022; published electronically August 22, 2022.

https://doi.org/10.1137/21M1452974

Funding: The work of the first author was supported by a Dahlquist Research Fellowship, funded by Comsol AB. The second author's work was financially supported by the European Union's Horizon 2020 research and innovation program under Marie Skłodowska-Curie grant 801133. The third author received support from the Research Council of Norway (NFR), grant 303362. The fourth author was supported by Research Council of Norway grants 300305 and 301013.

†KTH Royal Institute of Technology, Stockholm, Sweden (wietse@kth.se).

‡Department of Mathematics, University of Oslo, Oslo, Norway (timokoch@uio.no).

§Corresponding author. Simula Research Laboratory, Oslo, Norway (miroslav@simula.no).

¶Department of Mathematics, University of Oslo, Oslo, Norway, and Simula Research Laboratory, Oslo, Norway (kent-and@uio.no).

solved for at once) and domain-decomposition (DD) techniques (where the coupled system is solved using iterations between the subdomain problems). In the context of the primal Stokes–Darcy problem, which will be studied in this work, DD solvers have been established, e.g., in [27, 29, 26, 22, 21]. Monolithic solvers have been developed primarily for the nonsymmetric problem formulation in terms of Krylov solvers (GMRes) with block-diagonal and triangular preconditioners [20] or constrained indefinite preconditioners [23]. However, existing solvers are typically robust only in certain parameter regimes (cf. [20, 23]) or rely on algorithmic parameters that may be difficult to tune (e.g., Robin parameters in DD [26]).

Monolithic methods are in particular popular in applications with more complex physics, e.g., [55, 3, 24, 1], for their property that the interface conditions are fulfilled up to numerical precision independent of tuning parameters, and the practical observation that monolithic schemes often outperform DD schemes in cases where the DD solver requires many subdomain iterations. This can also be the case if optimal DD parameters are unknown for the specific problem and parameters or costly to determine. For completeness, we mention that there are also works that successfully apply DD techniques for problems with more complex physics, e.g., [11].

In [14, 42, 52], robust solvers for the Stokes–Darcy problem with Darcy equation in mixed form (see, e.g., [50, 35]) are constructed. While the mixed form has the advantage in the finite element context of ensuring local mass conservation, the total number of degrees of freedom (dofs) is significantly reduced with the Darcy problem in the primal form. Finite volume schemes feature local mass conservation by construction in both cases.

In the following, we construct robust monolithic solvers for the primal Stokes–Darcy system. More precisely, by considering different discretizations of the coupling conditions, we derive three different symmetric formulations which are amenable to discretization by finite element methods (FEM) or finite volume methods (FVM). Well-posedness of the formulations is established within an abstract framework and consequently block-diagonal preconditioners are constructed by operator preconditioning [53]. A crucial component of the analysis is the formulation in terms of fractional norms on the interface between the subdomains. In turn, the proposed preconditioners utilize nonstandard and nonlocal operators. However, as the number of dofs on the interface is often small relative to the problem size, we demonstrate that the preconditioners are feasible also in practical applications.

Our work is structured as follows. In section 2, we state the governing equations and coupling conditions, introduce the three variational formulations considered in this work, and show in a motivating example that a simple idea based on standard norms does not lead to a parameter-robust preconditioner. An abstract theory is then developed in section 3 and applied to the different formulations. Numerical experiments showcasing robustness of the proposed preconditioners and their efficiency are presented and discussed in section 4.

2. Problem formulation. Let $\Omega_S, \Omega_D \subset \mathbb{R}^d$, $d \in \{2, 3\}$, be two nonoverlapping Lipschitz domains sharing a common interface $\Gamma = \partial\Omega_S \cap \partial\Omega_D \subset \mathbb{R}^{d-1}$. Let Ω_D represent a porous medium in which we consider Darcy flow in primal form, i.e., formulated solely in terms of pressure p_D,

$$\nabla\cdot\left(-\mu^{-1}\boldsymbol{K}\nabla p_D\right) = f_D, \tag{2.1}$$

with constant fluid viscosity $\mu > 0$, and isotropic and homogeneous intrinsic permeability $\boldsymbol{K} = k\boldsymbol{I}$. For notational convenience, we further let $\kappa := \mu^{-1}k$.

In the free-flow domain Ω_S, we consider the Stokes problem,

$$-\nabla\cdot\boldsymbol{\sigma}(\boldsymbol{u}_S,p_S)=\boldsymbol{f}_S, \tag{2.2a}$$

$$-\nabla\cdot\boldsymbol{u}_S=0, \tag{2.2b}$$

with $\boldsymbol{\sigma}(\boldsymbol{u}_S,p_S)=2\mu\boldsymbol{\epsilon}(\boldsymbol{u}_S)-p_S\boldsymbol{I}$ and $\boldsymbol{\epsilon}(\boldsymbol{u}_S)=\frac{1}{2}\left(\nabla\boldsymbol{u}_S+\nabla\boldsymbol{u}_S{}^T\right)$.

To couple the Stokes and Darcy systems, let $\boldsymbol{n}:=\boldsymbol{n}_S$ be the outer normal of the Stokes domain and let $\boldsymbol{\tau}:=\boldsymbol{I}-(\boldsymbol{n}\otimes\boldsymbol{n})$ be the projection onto the tangent bundle of the interface. The following conditions are then assumed to hold on the interface Γ:

$$\boldsymbol{\tau}\cdot\boldsymbol{\sigma}(\boldsymbol{u}_S,p_S)\cdot\boldsymbol{n}+\beta_\tau\boldsymbol{\tau}\cdot\boldsymbol{u}_S=\boldsymbol{0}, \tag{2.3a}$$

$$\boldsymbol{n}\cdot\boldsymbol{\sigma}(\boldsymbol{u}_S,p_S)\cdot\boldsymbol{n}+p_D=0, \tag{2.3b}$$

$$\boldsymbol{n}\cdot\boldsymbol{u}_S+\boldsymbol{n}\cdot\kappa\nabla p_D=0. \tag{2.3c}$$

Here, the first of the coupling conditions is the well-established Beavers–Joseph–Saffman (BJS) condition [9, 63, 54] with $\beta_\tau:=\frac{\mu\alpha}{\sqrt{k}}$, and constant $\alpha\geq 0$. Finally, conditions (2.3b)–(2.3c) enforce normal stress continuity and mass conservation.

To close the coupled problem (2.1)–(2.3), we prescribe the following (homogeneous) boundary conditions:

$$\boldsymbol{u}_S=0 \quad \text{on } \Gamma_S^{\boldsymbol{u}}, \qquad \boldsymbol{n}_S\cdot\boldsymbol{\sigma}(\boldsymbol{u}_S,p_S)=0 \quad \text{on } \Gamma_S^{\boldsymbol{\sigma}}\neq\emptyset, \tag{2.4a}$$

$$-\boldsymbol{n}_D\cdot\kappa\nabla p_D=0 \quad \text{on } \Gamma_D^{u}, \qquad p_D=0 \quad \text{on } \Gamma_D^{p}\neq\emptyset. \tag{2.4b}$$

Here, we assume that $\Gamma_S^u\cup\Gamma_S^{\boldsymbol{\sigma}}\cup\Gamma$ forms a disjoint decomposition of $\partial\Omega_S$ and, analogously, $\Gamma_D^{\boldsymbol{u}}\cup\Gamma_D^p\cup\Gamma$ is a disjoint partition of $\partial\Omega_D$. Since we assume that both $\Gamma_S^{\boldsymbol{\sigma}}$ and Γ_D^p have positive measure, Γ cannot be a closed surface (or curve in two dimensions). In turn, we make the assumption that its boundary touches the boundary sections on which Stokes stress and Darcy flux boundary conditions are imposed, i.e., $\partial\Gamma\subseteq\partial\Gamma_S^{\boldsymbol{\sigma}}\cup\partial\Gamma_D^u$. These assumptions are made specifically to simplify the analysis in section 3 and will be relaxed in the numerical experiments of section 4.

2.1. Three variational formulations. In this work, we focus on three different formulations of the coupled problem (2.1)–(2.4). The formulations differ in the manner in which the flux continuity condition (2.3c) is incorporated. The first uses the trace of p_D on the interface to enforce this condition and we call this formulation the *Trace* (Tr) formulation. The second formulation uses the interface pressure as a Lagrange multiplier to enforce flux continuity and is therefore referred to as the *Lagrange multiplier* (La) system. Finally, the third system uses a Robin-type of interface condition and is thus called the *Robin* (Ro) formulation.

Each system is presented herein as a variational formulation posed in (subspaces of) spaces of square integrable functions. We assume that the spaces possess sufficient regularity for the (differential) operators in the systems to be well-defined. However, we reserve the precise definitions of these function spaces for a later stage since these require appropriately weighted norms.

The first formulation follows the classic derivation of [27]. Here, it is assumed that the pressure p_D has sufficient regularity for its trace on Γ to be well-defined. The weak form of (2.1)–(2.4) yields the *Trace formulation*: Find $(\boldsymbol{u}_S,p_S,p_D)\in\boldsymbol{V}_S\times Q_S\times Q_D$ such that

$$
\begin{aligned}
(2\mu\boldsymbol{\epsilon}(\boldsymbol{u}_S),\boldsymbol{\epsilon}(\boldsymbol{v}_S))_{\Omega_S}+\beta_\tau(\boldsymbol{\tau}\cdot\boldsymbol{u}_S,\boldsymbol{\tau}\cdot\boldsymbol{v}_S)_\Gamma&\\
-(p_S,\nabla\cdot\boldsymbol{v}_S)_{\Omega_S}+(p_D,\boldsymbol{n}\cdot\boldsymbol{v}_S)_\Gamma=(\boldsymbol{f}_S,\boldsymbol{v}_S)_{\Omega_S}&\quad\forall\boldsymbol{v}_S\in\boldsymbol{V}_S,\\
-(\nabla\cdot\boldsymbol{u}_S,q_S)_{\Omega_S}=0&\quad\forall q_S\in Q_S,\\
(\boldsymbol{n}\cdot\boldsymbol{u}_S,q_D)_\Gamma-(\kappa\nabla p_D,\nabla q_D)_{\Omega_D}=(f_D,q_D)_{\Omega_D}&\quad\forall q_D\in Q_D.
\end{aligned}
\tag{2.5}
$$

Here, and throughout this work, we use $(f,g)_\Sigma := \int_\Sigma fg$. We employ the same notation for vector and tensor-valued functions defined on a domain Σ.

Problem (2.5) can be naturally discretized by (H^1-)conforming finite element schemes, for example, the lowest-order Taylor–Hood ($\boldsymbol{P}_2$-P_1) pair for Stokes velocity and pressure and continuous piecewise quadratic Lagrange (P_2) elements for the Darcy pressure ($\boldsymbol{P}_2$-P_1-P_2 in the following).

The second formulation is motivated by cell-centered discretization methods including FVM and nonconforming FEM of lowest order. In that case, the trace of p_D is not (directly) available since there is no interfacial dof and it is common to use a discrete gradient reconstruction scheme to retrieve the interface pressure. To illustrate this, let us assume that the Darcy pressure space Q_D consists of piecewise constant functions. Introducing p_Γ as the unknown interface pressure, a two-point approximation (TPFA) of the flux on a facet $F\subset\Gamma$ reads

$$
-\boldsymbol{n}\cdot\kappa\nabla p_D := -\kappa\frac{p_D|_K-p_\Gamma}{h_K}\ \text{on } F,
\tag{2.6}
$$

where $p_D|_K$ denotes the pressure in the center of the element $K\subseteq\Omega_D$ with $F\subseteq\partial K$ and h_K is the distance between the centroids of K and F. We recall that $\boldsymbol{n}$ denotes the unit normal outward to Ω_S. Applying (2.6) in (2.3c) yields a discrete interface condition

$$
\boldsymbol{n}\cdot\boldsymbol{u}_S+\beta_n^{-1}(p_D|_K-p_\Gamma)=0\ \text{on } F
\tag{2.7}
$$

with $\beta_n := \kappa^{-1}h_K > 0$. Despite its motivation originating from the discrete case, we shall now consider β_n as a model parameter, allowing for a continuous formulation. In particular, we use (2.7) to model the flux continuity condition (2.3c) and arrive at the *Lagrange multiplier formulation*: Find $(\boldsymbol{u}_S,p_S,p_D,p_\Gamma)\in\boldsymbol{V}_S\times Q_S\times Q_D\times\Lambda$ such that

$$
\begin{aligned}
(2\mu\boldsymbol{\epsilon}(\boldsymbol{u}_S),\boldsymbol{\epsilon}(\boldsymbol{v}_S))_{\Omega_S}+\beta_\tau(\boldsymbol{\tau}\cdot\boldsymbol{u}_S,\boldsymbol{\tau}\cdot\boldsymbol{v}_S)_\Gamma&\\
-(p_S,\nabla\cdot\boldsymbol{v}_S)_{\Omega_S}+(p_\Gamma,\boldsymbol{n}\cdot\boldsymbol{v}_S)_\Gamma=(\boldsymbol{f}_S,\boldsymbol{v}_S)_{\Omega_S}&\quad\forall\boldsymbol{v}_S\in\boldsymbol{V}_S,\\
-(\nabla\cdot\boldsymbol{u}_S,q_S)_{\Omega_S}=0&\quad\forall q_S\in Q_S,\\
-(\kappa\nabla p_D,\nabla q_D)_{\Omega_D}-\left(\beta_n^{-1}\left(p_D-p_\Gamma\right),q_D\right)_\Gamma=(f_D,q_D)_{\Omega_D}&\quad\forall q_D\in Q_D,\\
(\boldsymbol{n}\cdot\boldsymbol{u}_S,q_\Gamma)_\Gamma+\left(\beta_n^{-1}\left(p_D-p_\Gamma\right),q_\Gamma\right)_\Gamma=0&\quad\forall q_\Gamma\in\Lambda.
\end{aligned}
\tag{2.8}
$$

By construction, this formulation is tailored for discretization methods that use cell-centered pressure variables. The precise discretization of the second-order terms $(2\mu\boldsymbol{\epsilon}(\boldsymbol{u}_S),\boldsymbol{\epsilon}(\boldsymbol{v}_S))_{\Omega_S}$ and $(\kappa\nabla p_D,\nabla q_D)_{\Omega_D}$ is presented in section SM1. Furthermore, we emphasize that only the specific choice of $\beta_n=\kappa^{-1}h_K$ leads to a discretization scheme that is consistent with (2.1)–(2.4).

Our third and final formulation is obtained by eliminating the Lagrange multiplier. For that, we once again consider a facet F with an adjacent cell $K\subseteq\Omega_D$.

The combination of the momentum balance (2.3b) with condition (2.7) yields a Robin-type interface condition

$$-\boldsymbol{n}\cdot\boldsymbol{\sigma}(\boldsymbol{u}_S,p_S)\cdot\boldsymbol{n}=p_D|_K+\beta_n\boldsymbol{u}_S\cdot\boldsymbol{n}\ \text{on}\ F. \tag{2.9}$$

By using (2.9) to model flux continuity, we arrive at the *Robin formulation*: Find $(\boldsymbol{u}_S,p_S,p_D)\in\boldsymbol{V}_S\times Q_S\times Q_D$ such that

$$\begin{aligned}
(2\mu\boldsymbol{\epsilon}(\boldsymbol{u}_S),\boldsymbol{\epsilon}(\boldsymbol{v}_S))_{\Omega_S}+\beta_\tau(\boldsymbol{\tau}\cdot\boldsymbol{u}_S,\boldsymbol{\tau}\cdot\boldsymbol{v}_S)_\Gamma&\\
+\beta_n(\boldsymbol{n}\cdot\boldsymbol{u}_S,\boldsymbol{n}\cdot\boldsymbol{v}_S)_\Gamma&\\
-(p_S,\nabla\cdot\boldsymbol{v}_S)_{\Omega_S}+(p_D,\boldsymbol{n}\cdot\boldsymbol{v}_S)_\Gamma=(\boldsymbol{f}_S,\boldsymbol{v}_S)_{\Omega_S}&\quad\forall\boldsymbol{v}_S\in\boldsymbol{V}_S,\\
-(\nabla\cdot\boldsymbol{u}_S,q_S)_{\Omega_S}=0&\quad\forall q_S\in Q_S,\\
(\boldsymbol{n}\cdot\boldsymbol{u}_S,q_D)_\Gamma-(\kappa\nabla p_D,\nabla q_D)_{\Omega_D}=(f_D,q_D)_{\Omega_D}&\quad\forall q_D\in Q_D.
\end{aligned} \tag{2.10}$$

Similar to (3.3), this formulation is amenable to cell-centered finite volume or nonconforming finite element methods. We emphasize that although variational formulations are more common for finite element practitioners, these final two systems can be interpreted term by term using finite volume discretization techniques.

2.2. Motivating example. Having defined the variational problems, our aim is to construct parameter-robust solvers for all three formulations. By robustness, we mean that the preconditioned system has a bounded eigenvalue spectrum independent of modeling and discretization parameters, in particular μ, κ, β_τ, the discretization length h, and the Robin coefficient β_n. We base our approach on operator preconditioning using nonstandard, weighted Sobolev spaces.

To illustrate the necessity of these techniques, let us first illustrate that a naïve but seemingly sensible approach in standard norms does not yield parameter-robustness. More precisely, in Example 2.1 we show that natural norms of the solution spaces of the coupled Stokes–Darcy problem do not translate to robust preconditioners.

Example 2.1 (standard norm preconditioner). We consider the Trace formulation (2.5) on $\Omega_S=[0,1]\times[1,2]$ and $\Omega_D=[0,1]\times[0,1]$ with the source terms $\boldsymbol{f}_S$, f_D defined in (A.2) and artificially balanced (nonzero right-hand side) coupling conditions (A.3) (see Appendix A for details). We let $\Gamma_S^{\boldsymbol{u}}$ be the top edge of Ω_S while the bottom edge of Ω_D is Γ_D^p. On the remaining parts of the boundaries, Neumann boundary conditions are assumed, i.e., traction for the Stokes and normal flux for the Darcy problem. The boundary conditions are nonhomogeneous with the data based on the manufactured exact solution (A.1).

Since (2.5) with the above boundary conditions is well-posed in $\boldsymbol{V}_S=\boldsymbol{H}^1_{0,\Gamma_S^{\boldsymbol{u}}}(\Omega_D)$, $Q_S=L^2(\Omega_D)$, and $Q_D=H^1_{0,\Gamma_D^p}(\Omega_D)$ (see [27]), we may want to consider as preconditioner the block-diagonal operator

$$\mathcal{B}:=\begin{bmatrix}-\nabla\cdot(2\mu\boldsymbol{\epsilon})+\beta_\tau T_\tau' T_\tau & & \\ & (2\mu)^{-1}I & \\ & & -\kappa\Delta\end{bmatrix}^{-1}, \tag{2.11}$$

where $T_\tau:\boldsymbol{V}_S\to\boldsymbol{V}_S'$ is the tangential trace operator. We remark that (2.11) is the Riesz map with respect to the parameter-weighted inner products of $\boldsymbol{V}_S\times Q_S\times Q_D$, which for $\mu=1$, $k=1$, $\beta_\tau=0$ reduce to standard inner products of the spaces. In particular, for the first block of (2.11), we recall that the first Korn inequality holds as $|\Gamma_S^{\boldsymbol{u}}|>0$.

TABLE 1

Performance of block-diagonal preconditioner (2.11) *for the Trace formulation of Stokes–Darcy problem* (2.5) *discretized by* $\boldsymbol{P}_2$-P_1-P_2 *elements. Setup of Example* 2.1 *and* $\mu = 1$. *Discretization length scale is denoted by* h. *This naïve preconditioner is sensitive to variations in permeability* k.

	$\alpha = 1$				$\alpha = 0$			
k \ h	2^{-4}	2^{-5}	2^{-6}	2^{-7}	2^{-4}	2^{-5}	2^{-6}	2^{-7}
1	34	33	32	32	34	33	32	32
10^{-1}	39	39	39	37	39	41	39	39
10^{-2}	52	52	50	49	55	56	54	53
10^{-3}	84	84	82	82	95	90	89	88
10^{-4}	165	186	184	187	181	202	205	200

Using discrete spaces $\boldsymbol{V}_{S,h} \subseteq \boldsymbol{V}_S$, $Q_{S,h} \subseteq Q_S$, $Q_{D,h} \subseteq Q_D$ constructed respectively with $\boldsymbol{P}_2$, P_1, and P_2 elements we investigate robustness of (2.11) by considering boundedness of preconditioned MinRes iterations with mesh refinement and parameter variations. The iterative solver is started from an initial vector representing a random function in $\boldsymbol{V}_{S,h} \times Q_{S,h} \times Q_{D,h}$ (implying that the dofs associated with the Dirichlet boundary conditions are set to 0, while the remaining dofs are drawn randomly from $[0, 1)$) and terminates once the preconditioned residual norm is reduced by factor 10^8. The preconditioner is computed by LU decomposition.

In Table 1, we report the number of MinRes iterations required to satisfy the convergence criteria. We observe that the iterations are stable in mesh size. However, there is a clear dependence on permeability and the iterations grow with decreasing k. The BJS parameter (or β_τ) seems to have little effect on the solver convergence.

We conclude that even though the blocks of (2.11) define parameter-robust preconditioners for the individual Stokes and Darcy subproblems this property is not sufficient for parameter-robustness in the coupled Stokes–Darcy problem.

Following this introductory example in which full parameter-robustness could not be achieved, parameter-robust preconditioners for all presented formulations of the Stokes–Darcy problem will be constructed using a unified framework introduced next.

3. Abstract setting. We observe that each of the three formulations (2.5), (2.8), and (2.10) presented in section 2.1 possesses a symmetric structure. Furthermore, the three systems can be identified as perturbed saddle point problems and we detail this observation in this section. To fully exploit this identification, we present an abstract theory of well-posedness for such problems. After introducing the used notation conventions, the main abstract result is shown and the three systems are each presented and analyzed in this functional framework.

3.1. Notation and preliminaries. We start with an exposition of notation conventions. For a bounded domain $\Omega \subset \mathbb{R}^d$, we let $L^2(\Omega)$ denote the space of square integrable functions and let $H^k(\Omega)$, $k \geq 1$, be the usual Sobolev space of functions with integer derivatives up to order k in $L^2(\Omega)$. Homogeneous boundary conditions on $\Gamma \subseteq \partial\Omega$ are indicated using a subscript 0, i.e., $H^1_{0,\Gamma}(\Omega) := \{f \in H^1(\Omega) \mid f = 0 \text{ on } \Gamma\}$. Vector-valued functions and their corresponding spaces are denoted by bold font.

The trace space of $H^1(\Omega)$ on Γ corresponds to $H^{\frac{1}{2}}(\Gamma)$, the interpolation space between $L^2(\Gamma)$ and $H^1(\Gamma)$. Its dual is denoted by $H^{-\frac{1}{2}}(\Gamma)$. More generally, we let X' be the dual of a Hilbert space X and let angled brackets $\langle \cdot, \cdot \rangle_{X',X}$ denote the duality pairing. The subscript on this pairing may be omitted when no confusion arises.

$\|\cdot\|_{k,\Omega}$ denotes the norm on $H^k(\Omega)$ and $\|\cdot\|_\Omega := \|\cdot\|_{0,\Omega}$. A weighted space αX with $\alpha > 0$ is endowed with the norm $\|f\|_{\alpha X} := \|\alpha f\|_X$ and its dual is given by $(\alpha X)' = \alpha^{-1} X'$. Moreover, given two Hilbert spaces X, Y, the intersection $(X \cap Y)$ and sum $(X + Y)$ form Hilbert spaces endowed with the norms

$$\|f\|^2_{X\cap Y} := \|f\|^2_X + \|f\|^2_Y, \qquad \|f\|^2_{X+Y} := \inf_{g\in Y} \left(\|f-g\|^2_X + \|g\|^2_Y\right),$$

respectively. Moreover, we recall the following relations [10]:

$$(X \cap Y)' = X' + Y', \qquad X \cap (Y_1 + Y_2) = (X \cap Y_1) + (X \cap Y_2).$$

Finally, the relation $x \lesssim y$ implies that a positive constant $c \in \mathbb{R}$ exists, independent of model parameters, such that $x \le cy$.

3.2. Well-posedness theory of perturbed saddle point problems. Let V and Q be Hilbert spaces to be specified below. Let $\mathcal{A} : V \times Q \to (V \times Q)'$ be a linear operator of the form

$$\mathcal{A} := \begin{bmatrix} A & B' \\ B & -C \end{bmatrix}, \tag{3.1}$$

in which the operators A, B, and C are subject to the following assumptions:

- Let $A : V \to V'$ be such that $\langle Au, v\rangle$ forms an inner product on V. We denote the induced norm by

  $$\|v\|^2_A := \langle Av, v\rangle \qquad \forall v \in V. \tag{3.2a}$$

- Let $B : V \to Q'$ be a linear operator and let $|\cdot|_B$ be a seminorm on Q such that B is continuous in the following sense:

  $$\langle Bv, p\rangle \lesssim \|v\|_A |p|_B \qquad \forall (v, p) \in V \times Q. \tag{3.2b}$$

  Moreover, we assume that a constant $\zeta_0 > 0$ exists such that for each $p \in Q$, a $v^p \in V$ exists that satisfies

  $$\langle Bv^p, p\rangle = |p|^2_B, \qquad \zeta_0 \|v^p\|_A \le |p|^2_B. \tag{3.2c}$$

  We refer to ζ_0 as the inf-sup constant.
- Let $C : Q \to Q'$ be such that $\langle Cp, q\rangle$ forms a semi-inner product on Q. The induced seminorm is denoted as

  $$|q|^2_C := \langle Cq, q\rangle \qquad \forall q \in Q. \tag{3.2d}$$

- Finally, we assume that

  $$|||(u, p)|||^2 := \|u\|^2_A + |p|^2_B + |p|^2_C \tag{3.2e}$$

  is a proper norm and we let $V \times Q$ be the space of (pairs of) measurable functions that are bounded in this norm.

The model problem of interest then reads, Given $(f, g) \in (V \times Q)'$, find $(u, p) \in V \times Q$ such that

$$\mathcal{A}(u, p) = (f, g). \tag{3.3}$$

Problem (3.3) is well-posed in $V \times Q$, as was shown in [16, Thm. 2]. Nevertheless, to have a self-contained presentation, we continue by demonstrating a simplified proof of this result in which we exploit the coercivity. We remark that in the above norms, the only constant that appears in the lower-bound is the inf-sup constant.

THEOREM 3.1. *If conditions* (3.2) *are fulfilled, then the saddle point problem* (3.3) *is well-posed in* $V \times Q$*, endowed with the norm* (3.2e).

Proof. We first show that $\mathcal{A}$ is continuous. By the Cauchy–Schwarz inequality, we have

$$\langle Au, v\rangle \le \|u\|_A \|v\|_A \qquad \forall u, v \in V,$$
$$\langle Cp, q\rangle \le |p|_C |q|_C \qquad \forall p, q \in Q.$$

Finally, condition (3.2b) ensures that B is continuous in the norm (3.2e). The combination of these three inequalities provides the continuity of $\mathcal{A}$. Since the operator $\mathcal{A}$ is linear and symmetric, it now suffices to show that ξ exists such that

$$\inf_{(u,p)} \sup_{(v,q)} \frac{\langle \mathcal{A}(u,p), (v,q)\rangle}{|||(u,p)||| \, |||(v,q)|||} \ge \xi > 0. \tag{3.4}$$

Let $(u,p) \in V \times Q$ be given and let us proceed by constructing a suitable test function $(v,q) \in V \times Q$. First, the condition (3.2c) allows us to construct $v^p \in V$ such that

$$\langle Bv^p, p\rangle = |p|_B^2, \qquad \zeta_0 \|v^p\|_A \le |p|_B. \tag{3.5}$$

Now let $(v,q) := (u + \zeta_0^2 v^p, -p)$ with ζ_0 from (3.2c). Substituting these definitions, we obtain

$$\begin{aligned} \langle \mathcal{A}(u,p), (v,q)\rangle &= \langle Au, v\rangle + \langle Bv, p\rangle + \langle Bu, q\rangle - \langle Cp, q\rangle \\ &= \|u\|_A^2 + \langle Au, \zeta_0^2 v^p\rangle + \langle B\zeta_0^2 v^p, p\rangle + |p|_C^2 \\ &= \|u\|_A^2 + \zeta_0^2 \langle Au, v^p\rangle + \zeta_0^2 |p|_B^2 + |p|_C^2. \end{aligned} \tag{3.6}$$

Next, we need to bound the second term in the right-hand side from below. Using the Cauchy–Schwarz inequality, the inequality $2ab \le a^2 + b^2$, and (3.5), we derive

$$\begin{aligned} \zeta_0^2 \langle Au, v^p\rangle &\ge -\zeta_0^2 \|u\|_A \|v^p\|_A \\ &\ge -\frac{1}{2}\|u\|_A^2 - \frac{1}{2}\zeta_0^4 \|v^p\|_A^2 \\ &\ge -\frac{1}{2}\|u\|_A^2 - \frac{1}{2}\zeta_0^2 |p|_B^2. \end{aligned} \tag{3.7}$$

In turn, (3.6) and (3.7) imply

$$\langle \mathcal{A}(u,p), (v,q)\rangle \ge \frac{1}{2}\|u\|_A^2 + \frac{1}{2}\zeta_0^2 |p|_B^2 + |p|_C^2 \ge \frac{\min\{1, \zeta_0^2\}}{2} |||(u,p)|||^2. \tag{3.8}$$

Next, we show that (v,q) is bounded in the norm (3.2e) by (u,p):

$$\begin{aligned} |||(v,q)|||^2 &= \|u + \zeta_0^2 v^p\|_A^2 + |p|_B^2 + |p|_C^2 \\ &\le 2\|u\|_A^2 + 2\|\zeta_0^2 v^p\|_A^2 + |p|_B^2 + |p|_C^2 \\ &\le 2\|u\|_A^2 + (1 + 2\zeta_0^2)|p|_B^2 + |p|_C^2 \\ &\le \max\{2, 1 + 2\zeta_0^2\} |||(u,p)|||^2. \end{aligned} \tag{3.9}$$

Combining (3.8) and (3.9), we have

$$\frac{\langle \mathcal{A}(u,p), (v,q)\rangle}{|||(u,p)||| \, |||(v,q)|||} \ge \frac{\min\{1, \zeta_0^2\}}{2\sqrt{\max\{2, 1 + 2\zeta_0^2\}}} > 0.$$

The Banach–Nečas–Babuška theorem [31, Thm. 2.6] then provides the result. ∎

Remark 3.1. Systems similar to (3.3) were recently considered in [43, 15], in which A is assumed to be coercive on the kernel of B. Since we herein make the stronger assumption of coercivity on the entire space V, Theorem 3.1 is corollary to [43, Thm. 5] and [15, Thm. 2.1].

At this point, we are ready to analyze the individual Stokes–Darcy formulations within the introduced abstract framework.

3.3. The Trace formulation. Observe that the left-hand side of (2.5) defines an operator $\mathcal{A}^{\mathrm{Tr}}$ on $\boldsymbol{V}_S \times (Q_S \times Q_D)$,

$$\mathcal{A}^{\mathrm{Tr}} := \begin{bmatrix} -\nabla\cdot(2\mu\boldsymbol{\epsilon}) + \beta_\tau T_\tau' T_\tau & \nabla & T_n' \\ -\nabla\cdot & & \\ T_n & & \kappa\Delta \end{bmatrix}, \tag{3.10}$$

where $T_\tau : \boldsymbol{V}_S \to V_S'$ is the tangential trace operator, and $T_n : \boldsymbol{V}_S \to Q_D'$ is the normal trace operator. The system thus fits template (3.1) of a perturbed saddle point problem with

$$\begin{aligned} \langle A\boldsymbol{u}_S, \boldsymbol{v}_S\rangle &:= (2\mu\boldsymbol{\epsilon}(\boldsymbol{u}_S), \boldsymbol{\epsilon}(\boldsymbol{v}_S))_{\Omega_S} + \beta_\tau(\boldsymbol{\tau}\cdot\boldsymbol{u}_S, \boldsymbol{\tau}\cdot\boldsymbol{v}_S)_\Gamma, \\ \langle B\boldsymbol{u}_S, (q_S, q_D)\rangle &:= -(\nabla\cdot\boldsymbol{u}_S, q_S)_{\Omega_S} + (\boldsymbol{n}\cdot\boldsymbol{u}_S, q_D)_\Gamma, \\ \langle C(p_S, p_D), (q_S, q_D)\rangle &:= (\kappa\nabla p_D, \nabla q_D)_{\Omega_D}. \end{aligned}$$

Based on these operators, we define the following (semi-)norms:

$$\|\boldsymbol{u}_S\|_A^2 := 2\mu\|\boldsymbol{\epsilon}(\boldsymbol{u}_S)\|_{\Omega_S}^2 + \beta_\tau\|\boldsymbol{\tau}\cdot\boldsymbol{u}_S\|_\Gamma^2, \tag{3.11a}$$

$$|(p_S, p_D)|_B^2 := (2\mu)^{-1}\|p_S\|_{\Omega_S}^2 + (2\mu)^{-1}\|p_D\|_{-\frac{1}{2},\Gamma}^2, \tag{3.11b}$$

$$|(p_S, p_D)|_C^2 := \kappa\|\nabla p_D\|_{\Omega_D}^2. \tag{3.11c}$$

Finally, in the context of Theorem 3.1, we consider the following norm:

$$\begin{aligned} |||(\boldsymbol{u}_S, p_S, p_D)|||^2 := {} & 2\mu\|\boldsymbol{\epsilon}(\boldsymbol{u}_S)\|_{\Omega_S}^2 + \beta_\tau\|\boldsymbol{\tau}\cdot\boldsymbol{u}_S\|_\Gamma^2 \\ & + (2\mu)^{-1}\|p_S\|_{\Omega_S}^2 + (2\mu)^{-1}\|p_D\|_{-\frac{1}{2},\Gamma}^2 + \kappa\|\nabla p_D\|_{\Omega_D}^2. \end{aligned} \tag{3.12}$$

THEOREM 3.2. *Problem* (2.5) *is well-posed in* $V \times Q$ *endowed with the norm* (3.12).

Proof. We follow the assumptions of Theorem 3.1. First, the properties (3.2a) and (3.2d) are immediately fulfilled. Next, the continuity of B (3.2b) is shown by the following calculation, utilizing the Cauchy–Schwarz inequality and a trace inequality:

$$\begin{aligned} \langle B\boldsymbol{u}_S, (p_S, p_D)\rangle &= -(\nabla\cdot\boldsymbol{u}_S, p_S)_{\Omega_S} + (\boldsymbol{n}\cdot\boldsymbol{u}_S, p_D)_\Gamma \\ &\le \|\nabla\cdot\boldsymbol{u}_S\|_{\Omega_S}\|p_S\|_{\Omega_S} + \|\boldsymbol{n}\cdot\boldsymbol{u}_S\|_{\frac{1}{2},\Gamma}\|p_D\|_{-\frac{1}{2},\Gamma} \\ &\lesssim \|\boldsymbol{\epsilon}(\boldsymbol{u}_S)\|_{\Omega_S}\left(\|p_S\|_{\Omega_S} + \|p_D\|_{-\frac{1}{2},\Gamma}\right) \\ &\lesssim (2\mu)^{\frac{1}{2}}\|\boldsymbol{\epsilon}(\boldsymbol{u}_S)\|_{\Omega_S}(2\mu)^{-\frac{1}{2}}\left(\|p_S\|_{\Omega_S}^2 + \|p_D\|_{-\frac{1}{2},\Gamma}^2\right)^{\frac{1}{2}} \\ &= \|\boldsymbol{u}_S\|_A|(p_S, p_D)|_B. \end{aligned}$$

Condition (3.2c) on B is considered next. Let (p_S, p_D) be given. Let $\boldsymbol{v}^{p_S} \in \boldsymbol{H}^1(\Omega_S)$ be constructed, using the Stokes inf-sup condition, such that

$$\boldsymbol{v}^{p_S}|_\Gamma = 0, \qquad \nabla \cdot \boldsymbol{v}^{p_S} = -p_S, \tag{3.13a}$$

$$\|\boldsymbol{\epsilon}(\boldsymbol{v}^{p_S})\|_{\Omega_S} \lesssim \|p_S\|_{\Omega_S}. \tag{3.13b}$$

On the other hand, let $\phi \in H^{\frac{1}{2}}(\Gamma)$ be the Riesz representative of $p_D|_\Gamma \in H^{-\frac{1}{2}}(\Gamma)$. We then define $\boldsymbol{v}^{p_D} \in \boldsymbol{H}^1(\Omega_S)$ as the bounded extension that satisfies

$$\boldsymbol{v}^{p_D}|_\Gamma = \phi \boldsymbol{n}, \qquad \nabla \cdot \boldsymbol{v}^{p_D} = 0, \tag{3.14a}$$

$$\|\boldsymbol{\epsilon}(\boldsymbol{v}^{p_D})\|_{\Omega_S} \lesssim \|\phi\|_{\frac{1}{2},\Gamma} = \|p_D\|_{-\frac{1}{2},\Gamma}. \tag{3.14b}$$

We are now ready to set the test function $\boldsymbol{v}_S := (2\mu)^{-1}(\boldsymbol{v}^{p_S} + \boldsymbol{v}^{p_D})$. Noting that $\boldsymbol{\tau} \cdot \boldsymbol{v}_S = 0$ on Γ, this function satisfies

$$\begin{aligned}
\langle B\boldsymbol{v}_S, (p_S, p_D)\rangle &= -(2\mu)^{-1}(\nabla \cdot \boldsymbol{v}^{p_S}, p_S)_{\Omega_D} + (2\mu)^{-1}(\boldsymbol{n} \cdot \boldsymbol{v}^{p_D}, p_D)_\Gamma \\
&= (2\mu)^{-1}\|p_S\|^2_{\Omega_S} + (2\mu)^{-1}\|p_D\|^2_{-\frac{1}{2},\Gamma} \\
&= |(p_S, p_D)|^2_B, \qquad (3.15a) \\
\|\boldsymbol{v}_S\|_A &= (2\mu)^{\frac{1}{2}}\|\boldsymbol{\epsilon}((2\mu)^{-1}(\boldsymbol{v}^{p_S} + \boldsymbol{v}^{p_D}))\|_{\Omega_S} \\
&\le (2\mu)^{-\frac{1}{2}}\left(\|\boldsymbol{\epsilon}(\boldsymbol{v}^{p_S})\|_{\Omega_S} + \|\boldsymbol{\epsilon}(\boldsymbol{v}^{p_D})\|_{\Omega_S}\right) \\
&\lesssim (2\mu)^{-\frac{1}{2}}\left(\|p_S\|_{\Omega_S} + \|p_D\|_{-\frac{1}{2},\Gamma}\right) \\
&\lesssim |(p_S, p_D)|_B. \qquad (3.15b)
\end{aligned}$$

Hence, condition (3.2c) is fulfilled.

Finally, it is straightforward to verify that (3.2e) is a norm on Q and thus the assumptions of Theorem 3.1 are fulfilled. ∎

Following operator preconditioning [53], and using the well-posedness result of Theorem 3.2, a preconditioner for the Stokes–Darcy in the Trace formulation (2.5) is the Riesz map with respect to the inner product inducing the norms (3.12), that is, the block diagonal operator

$$\mathcal{B}^{\mathrm{Tr}} := \begin{bmatrix} -\nabla \cdot (2\mu\boldsymbol{\epsilon}) + \beta_\tau T'_\tau T_\tau & & \\ & (2\mu)^{-1} I & \\ & & -\kappa\Delta + (2\mu)^{-1}\left(-\Delta_\Gamma\right)^{-1/2} \end{bmatrix}^{-1}. \tag{3.16}$$

Here, the subscript Γ signifies that the fractional operator acts on the interface. We demonstrate, numerically, robustness of the preconditioner (3.16) using both H^1-conforming and nonconforming Stokes–Darcy-stable elements in section 4. Here, we continue with the remaining two formulations concerning cell-centered finite volume schemes and lowest-order nonconforming finite element schemes.

3.4. The Lagrange multiplier formulation. Variational problem (2.8) defines an operator $\mathcal{A}^{\mathrm{La}}$ on $\boldsymbol{V}_S \times (Q_S \times Q_D \times \Lambda)$,

$$\mathcal{A}^{\mathrm{La}} := \begin{bmatrix} -\nabla \cdot (2\mu\boldsymbol{\epsilon}) + \beta_\tau T'_\tau T_\tau & \nabla & & T'_n \\ -\nabla \cdot & & & \\ & & \kappa\Delta - \beta_n^{-1} T'T & \beta_n^{-1} T' \\ T_n & & \beta_n^{-1} T & -\beta_n^{-1} I \end{bmatrix}, \tag{3.17}$$

where $T : Q_D \to \Lambda'$ is a trace/restriction operator for the Darcy pressure space. We observe that the lower 2×2 block forms a discretization of the Laplacian in terms of the interior Darcy pressure and the interface pressure. In this sense, (3.17) is similar to (3.10).

We note that the operator (3.17) also fits template (3.1) with the operators given by

$$\begin{aligned}\langle A\boldsymbol{u}_S, \boldsymbol{v}_S\rangle &:= (2\mu\boldsymbol{\epsilon}(\boldsymbol{u}_S), \boldsymbol{\epsilon}(\boldsymbol{v}_S))_{\Omega_S} + \beta_\tau(\boldsymbol{\tau}\cdot\boldsymbol{u}_S, \boldsymbol{\tau}\cdot\boldsymbol{v}_S)_\Gamma,\\ \langle B\boldsymbol{u}_S, (q_S, q_D, q_\Gamma)\rangle &:= -(\nabla\cdot\boldsymbol{u}_S, q_S)_{\Omega_S} + (\boldsymbol{n}\cdot\boldsymbol{u}_S, q_\Gamma)_\Gamma,\\ \langle C(p_S, p_D, p_\Gamma), (q_S, q_D, q_\Gamma)\rangle &:= (\kappa\nabla p_D, \nabla q_D)_{\Omega_D} + (\beta_n^{-1}(p_D - p_\Gamma), (q_D - q_\Gamma))_\Gamma.\end{aligned}$$

These operators lead us to the following norms:

$$\|\boldsymbol{u}_S\|_A^2 := 2\mu\|\boldsymbol{\epsilon}(\boldsymbol{u}_S)\|_{\Omega_S}^2 + \beta_\tau\|\boldsymbol{\tau}\cdot\boldsymbol{u}_S\|_\Gamma^2, \tag{3.18a}$$

$$|(p_S, p_D, p_\Gamma)|_B^2 := (2\mu)^{-1}\|p_S\|_{\Omega_S}^2 + (2\mu)^{-1}\|p_\Gamma\|_{-\frac{1}{2},\Gamma}^2, \tag{3.18b}$$

$$|(p_S, p_D, p_\Gamma)|_C^2 := \kappa\|\nabla p_D\|_{\Omega_D}^2 + \beta_n^{-1}\|p_D - p_\Gamma\|_\Gamma^2. \tag{3.18c}$$

THEOREM 3.3. *Problem* (3.17) *is well-posed in* $V \times Q$ *endowed with the energy norm* (3.2e) *formed by* (3.18).

Proof. Assumptions (3.2a) and (3.2d) are again immediate. Assumptions (3.2b) and (3.2c) were proven in Theorem 3.2 (with $p_D|_\Gamma$ substituted for p_Γ). Then, Theorem 3.1 provides the result. ∎

Following Theorem 3.3, a preconditioner for problem (2.8) reads

$$\mathcal{B}^{\mathrm{La}} := \begin{bmatrix} -\nabla\cdot(2\mu\boldsymbol{\epsilon}) + \beta_\tau T_\tau' T_\tau & & & \\ & (2\mu)^{-1} I & & \\ & & -\kappa\Delta + \beta_n^{-1} T'T & -\beta_n^{-1} T' \\ & & -\beta_n^{-1} T & \beta_n^{-1} I_\Gamma + (2\mu)^{-1}(-\Delta_\Gamma)^{-1/2} \end{bmatrix}^{-1}. \tag{3.19}$$

Finally, we consider the third variational form established by eliminating the Lagrange multiplier on the coupling interface.

3.5. The Robin formulation. We observe that problem (2.10) is given in terms of the operator $\mathcal{A}^{\mathrm{Ro}}$ on $\boldsymbol{V}_S \times (Q_S \times Q_D)$

$$\mathcal{A}^{\mathrm{Ro}} := \begin{bmatrix} -\nabla\cdot(2\mu\boldsymbol{\epsilon}) + \beta_\tau T_\tau' T_\tau + \beta_n T_n' T_n & \nabla & T_n' \\ -\nabla\cdot & & \\ T_n & & \kappa\Delta \end{bmatrix}. \tag{3.20}$$

Note again that (3.20) has the structure (3.1) with the operators given by

$$\begin{aligned}\langle A\boldsymbol{u}_S, \boldsymbol{v}_S\rangle &:= (2\mu\boldsymbol{\epsilon}(\boldsymbol{u}_S), \boldsymbol{\epsilon}(\boldsymbol{v}_S))_{\Omega_S}\\ &\quad + \beta_\tau(\boldsymbol{\tau}\cdot\boldsymbol{u}_S, \boldsymbol{\tau}\cdot\boldsymbol{v}_S)_\Gamma + \beta_n(\boldsymbol{n}\cdot\boldsymbol{u}_S, \boldsymbol{n}\cdot\boldsymbol{v}_S)_\Gamma,\\ \langle B\boldsymbol{u}_S, (q_S, q_D)\rangle &:= -(\nabla\cdot\boldsymbol{u}_S, q_S)_{\Omega_S} + (\boldsymbol{n}\cdot\boldsymbol{u}_S, q_D)_\Gamma,\\ \langle C(p_S, p_D), (q_S, q_D)\rangle &:= (\kappa\nabla p_D, \nabla q_D)_{\Omega_D}.\end{aligned}$$

In the framework of Theorem 3.1, we identify the following norms:

$$\|\boldsymbol{u}_S\|_A^2 := 2\mu\|\boldsymbol{\epsilon}(\boldsymbol{u}_S)\|_{\Omega_S}^2 + \beta_\tau\|\boldsymbol{\tau}\cdot\boldsymbol{u}_S\|_\Gamma^2 + \beta_n\|\boldsymbol{n}\cdot\boldsymbol{u}_S\|_\Gamma^2, \tag{3.21a}$$

$$|(p_S, p_D)|_B^2 := (2\mu)^{-1}\|p_S\|_{\Omega_S}^2 + \|p_D\|^2_{(2\mu)^{-\frac{1}{2}}H^{-\frac{1}{2}}(\Gamma) + \beta_n^{-\frac{1}{2}}L^2(\Gamma)}, \tag{3.21b}$$

$$|(p_S, p_D)|_C^2 := \kappa\|\nabla p_D\|_{\Omega_D}^2. \tag{3.21c}$$

We remark that the control on the pressure variable is weakened in comparison with (3.18). This is a direct result from the fact that $\boldsymbol{u}_S$ is now in a smaller space (with a stronger norm).

THEOREM 3.4. *Problem* (3.20) *is well-posed in* $V \times Q$ *endowed with the energy norm formed by* (3.21).

Proof. Assumptions (3.2a) and (3.2d) follow immediately. We continue with the bounds on B, starting with continuity (3.2b):

$$\begin{aligned}\langle B\boldsymbol{u}_S, (q_S, q_D)\rangle &= -(\nabla\cdot\boldsymbol{u}_S, q_S)_{\Omega_S} + (\boldsymbol{n}\cdot\boldsymbol{u}_S, q_D)_\Gamma \\ &\le \|\boldsymbol{\epsilon}(\boldsymbol{u}_S)\|_{(2\mu)^{\frac12}L^2(\Omega_S)}\|q_S\|_{(2\mu)^{-\frac12}L^2(\Omega_S)} \\ &\quad + \|\boldsymbol{n}\cdot\boldsymbol{u}_S\|_{(2\mu)^{\frac12}H^{\frac12}(\Gamma)\cap\beta_n^{\frac12}L^2(\Gamma)}\|q_D\|_{(2\mu)^{-\frac12}H^{-\frac12}(\Gamma)+\beta_n^{-\frac12}L^2(\Gamma)} \\ &\lesssim \|\boldsymbol{u}_S\|_A + |(q_S, q_D)|_B,\end{aligned}$$

in which we used that $(cX)' = c^{-1}X'$ for $c > 0$ and $(X\cap Y)' = X + Y$; cf. section 3.1.

Second, we prove condition (3.2c) for which we follow the same approach as in Theorem 3.2. Let (p_S, p_D) be given with bounded B-seminorm and let $\boldsymbol{v}^{p_S}$ satisfy (3.13). For notational convenience, we define

$$\Lambda := (2\mu)^{\frac12}H^{\frac12}(\Gamma)\cap\beta_n^{\frac12}L^2(\Gamma), \qquad \Lambda' := (2\mu)^{-\frac12}H^{-\frac12}(\Gamma) + \beta_n^{-\frac12}L^2(\Gamma). \tag{3.22}$$

Now, let $\phi\in\Lambda$ be the Riesz representative of $p_D|_\Gamma \in \Lambda'$. Since $\Lambda\subseteq H^{\frac12}(\Gamma)$, we can define $\boldsymbol{v}^{p_D}\in\boldsymbol{H}^1(\Omega_S)$ according to (3.14). This function satisfies the bound $\|\boldsymbol{\epsilon}(\boldsymbol{v}^{p_D})\|_{\Omega_S}\lesssim\|\phi\|_{\frac12,\Gamma}$ and we obtain

$$\begin{aligned}\|(2\mu)^{\frac12}\boldsymbol{\epsilon}(\boldsymbol{v}^{p_D})\|_{\Omega_S}^2 + \|\beta_n^{\frac12}\boldsymbol{n}\cdot\boldsymbol{v}^{p_D}\|_\Gamma^2 &\lesssim \|(2\mu)^{\frac12}\phi\|_{\frac12,\Gamma}^2 + \|\beta_n^{\frac12}\phi\|_\Gamma^2 \\ &= \|\phi\|_\Lambda^2 = \|p_D\|_{\Lambda'}^2.\end{aligned}$$

Finally, we define the test function $\boldsymbol{v} = (2\mu)^{-1}\boldsymbol{v}^{p_S} + \boldsymbol{v}^{p_D}$ and deduce

$$\begin{aligned}\langle B\boldsymbol{v}_S, (p_S, p_D)\rangle &= -(2\mu)^{-1}(\nabla\cdot\boldsymbol{v}^{p_S}, p_S)_{\Omega_D} + (\boldsymbol{n}\cdot\boldsymbol{v}^{p_D}, p_D)_\Gamma \\ &= (2\mu)^{-1}\|p_S\|_{\Omega_S}^2 + \|p_D\|_{\Lambda'}^2 \\ &= |(p_S, p_D)|_B^2, \qquad (3.23a)\\ \|\boldsymbol{v}_S\|_A^2 &= (2\mu)\|\boldsymbol{\epsilon}((2\mu)^{-1}\boldsymbol{v}^{p_S} + \boldsymbol{v}^{p_D})\|_{\Omega_S}^2 + \beta_n\|\boldsymbol{n}\cdot\boldsymbol{v}^{p_D}\|_\Gamma^2 \\ &\lesssim (2\mu)^{-1}\|\boldsymbol{\epsilon}(\boldsymbol{v}^{p_S})\|_{\Omega_S}^2 + \|(2\mu)^{\frac12}\boldsymbol{\epsilon}(\boldsymbol{v}^{p_D})\|_{\Omega_S}^2 + \|\beta_n^{\frac12}\boldsymbol{n}\cdot\boldsymbol{v}^{p_D}\|_\Gamma^2 \\ &\lesssim (2\mu)^{-\frac12}\|p_S\|_{\Omega_S}^2 + \|p_D\|_{\Lambda'}^2 \\ &= |(p_S, p_D)|_B^2. \qquad (3.23b)\end{aligned}$$

Now, (3.23) implies that assumption (3.2c) is fulfilled and the result follows by Theorem 3.1. ∎

Theorem 3.4 leads us to the preconditioner for the third formulation:

$$\mathcal{B}^{\mathrm{Ro}} = \begin{bmatrix} \begin{pmatrix} -\nabla\cdot(2\mu\boldsymbol{\epsilon}) + \beta_\tau T_\tau' T_\tau \\ +\beta_n T_n' T_n \end{pmatrix}^{-1} & & \\ & \left((2\mu)^{-1}I\right)^{-1} & \\ & & \begin{pmatrix} \left(-\kappa\Delta + \beta_n^{-1}I_\Gamma\right)^{-1} \\ +\left(-\kappa\Delta + (2\mu)^{-1}(-\Delta_\Gamma)^{-\frac12}\right)^{-1} \end{pmatrix} \end{bmatrix}. \tag{3.24}$$

Note that the (1×1) Darcy pressure block of the preconditioner contains a sum of two inverse operators. This construction is typical in preconditioning sums of spaces, as discussed in [6].

4. Numerical experiments. For finite element and finite volume discretizations, we let $\Omega_{i,h}$, $i = D, S$ (h being the characteristic discretization length) denote the meshes of Ω_D, Ω_S that conform to Γ in the sense that every facet F on the interface Γ satisfies $F = \partial K_D \cap \partial K_S$ for some unique cell pair $K_D \in \Omega_{D,h}$ and $K_S \in \Omega_{S,h}$. The mesh of the interface (consisting of facets F) is denoted by Γ_h.

Unless stated otherwise, the geometry setup and boundary data of Example 2.1 are used, i.e., $\Omega_S = [0,1] \times [1,2]$, $\Omega_D = [0,1] \times [0,1]$ with the source terms defined in (A.2) and the top edge of Ω_S and the bottom edge of Ω_D designated as Dirichlet boundaries $\Gamma_S^{\boldsymbol{u}}$, Γ_D^p, respectively. On the remaining boundaries, Neumann conditions are given. The nonhomogeneous boundary data matches (A.1). In all examples, the Krylov solver terminates when the preconditioned residual norm is reduced by a factor 10^8.

All numerical tests are implemented using the scientific software frameworks FEniCS$_{\text{ii}}$ [48] (FEM) and DuMu$^{\text{x}}$/DUNE [47, 8] (FVM), where we use PETSc [7], SLEPc [40] (FEM), and Eigen [39], and Spectra [59] (FVM) for solving exact and approximate generalized eigenvalue problems (discrete fractional Laplacian, condition numbers). The preconditioners are implemented within the abstract linear solver frameworks of PETSc (FEM) and dune-istl [13] (FVM).

Since the discretization of the preconditioners is not straightforward due to the interfacial contributions, we first provide some details regarding their construction in section 4.1. To demonstrate robustness of the proposed preconditioners, we conduct numerical experiments with large parameter ranges motivated by the practical applications and dimensional analysis discussed in section 4.2. Numerical results are finally presented in section 4.3.

4.1. Discrete preconditioners. The (only) nonstandard component common to all our Stokes–Darcy preconditioners is the fractional operator $\mu^{-1}(-\Delta_\Gamma)^{-1/2}$. Following [49], we consider here the approximation based on the spectral definition which requires solution of the following generalized eigenvalue problem in a discrete space $V_h = V_h(\Gamma_h)$, $n = \dim(V_h)$: For $1 \le i \le n$ find $(u_i, \lambda_i) \in V_h \times \mathbb{R}$ such that

$$(u_i, v)_{\mu^{-\frac{1}{2}} H^1(\Gamma)} = \lambda_i (u_i, v)_{\mu^{-\frac{1}{2}} L^2(\Gamma)} \quad \forall v \in V_h \tag{4.1}$$

with the orthogonality condition $(u_i, u_j)_{\mu^{-\frac{1}{2}} L^2(\Gamma)} = \delta_{ij}$. Then, we let

$$\langle \mu^{-1}(-\Delta_\Gamma)^{-1/2} u, v \rangle := \sum_i \lambda_i^{-1/2} (u_i, u)_{\mu^{-\frac{1}{2}} L^2(\Gamma)} (u_i, v)_{\mu^{-\frac{1}{2}} L^2(\Gamma)}, \quad u, v \in V_h. \tag{4.2}$$

We note that (4.1) is related to the weak formulation of $\mu^{-1}(-\Delta_\Gamma + I_\Gamma)u = \mu^{-1}\lambda u$ in Γ with Neumann boundary conditions[1] on the boundary $\partial\Gamma$.

Introducing matrices $\boldsymbol{A}_h$ (discrete $\mu^{-1}(-\Delta_\Gamma + I_\Gamma)$ operator), $\boldsymbol{M}_h$ (discrete $\mu^{-1} I_\Gamma$ operator), the matrix representation of (4.2) (with respect to the basis of V_h) reads

$$\boldsymbol{M}_h \boldsymbol{U}_h \boldsymbol{E}_h^{-1/2} \boldsymbol{U}_h^T \boldsymbol{M}_h^T, \text{ where } \boldsymbol{A}_h \boldsymbol{U}_h = \boldsymbol{M}_h \boldsymbol{U}_h \boldsymbol{E}_h \text{ and } \boldsymbol{U}_h^T \boldsymbol{M}_h \boldsymbol{U}_h = \boldsymbol{I}_h.$$

That is, $\boldsymbol{E}_h, \boldsymbol{U}_h \in \mathbb{R}^{n \times n}$ are the solutions of the eigenvalue problem (4.1) with the eigenvalues forming the entries of the diagonal matrix $\boldsymbol{E}_h$ and columns of $\boldsymbol{U}_h$ being

[1] The actual boundary data is irrelevant as it does not enter the operator.

the $\boldsymbol{M}_h$-orthonormal eigenvectors. We remark that for cell-centered finite volume and P_0 finite element discretizations $\boldsymbol{M}_h$ is a diagonal matrix.

While the eigenvalue problem makes the construction inefficient for large scale applications, it is suitable for our robustness investigations where, in particular, we are interested in exact preconditioners. For large scale applications, scalable realizations of the Darcy pressure preconditioners in (3.16), (3.19), and (3.24) are, to the best of the authors' knowledge, yet to be established. However, efficient solvers for the interfacial component alone, i.e., $\mu^{-1}(-\Delta_\Gamma)^{-1/2}$, are known, e.g., [57, 34, 17, 5, 69].

Concerning the discretization of (4.1), we note that we use the full H^1-inner product, since in Example 2.1 and as assumed in section 2, the interface Γ intersects Neumann boundaries (see [35, 42] for discussion of multiplier spaces in relation to the spaces/boundary conditions on the adjacent subproblems). For the case of Γ intersecting boundaries with Dirichlet conditions, we refer to section SM2.

Finally, let us note that while in the multiplier formulation (3.19) the trace space V_h for (4.1) is explicit, i.e., $V_h = \Lambda_h$, this is not the case for the preconditioners for the Trace and Robin formulations, (3.16) and (3.24). More precisely, to compute the approximation of

$$\left(-\kappa\Delta + (2\mu)^{-1}\left(-\Delta_\Gamma\right)^{-1/2}\right)^{-1}$$

a mapping $\Pi_\Gamma : Q_{D,h} \to V_h$ is required. In the following, Π_Γ is defined as an L^2 projection to V_h. That is, given $q_h \in Q_{D,h}$, we let $\Pi_\Gamma q_h = \operatorname{argmin}_{v_h \in V_h} \|v_h - q_h\|^2_{L^2(\Gamma)}$. For $\boldsymbol{P}_2$-P_1-P_2 discretization V_h is then constructed with P_2 elements. When using the Crouzeix–Raviart element in a $\boldsymbol{CR}_1$-P_0-P_0 discretization or the cell-centered finite volume discretization, the space V_h is constructed using P_0 elements.

Results of the numerical experiments presented in the subsequent sections shall demonstrate that the above spaces lead to stable discretizations. We remark that for this property the trace space cannot be chosen arbitrarily. For example, with the Taylor–Hood element the choice of P_0 for V_h violates the discrete inf-sup condition and in turn results in parameter sensitivity of the Trace formulation (2.5) with the preconditioner (3.16).

4.2. Relevant parameter ranges. Having specified the discretizations of preconditioners we identify next the parameter regimes for which robustness is investigated in numerical experiments. We chose the parameter ranges based on a scaling analysis and several real-life applications.

Let U_0 be the characteristic Stokes velocity magnitude, ΔP_0 the characteristic pressure difference in the Stokes domain, and L_0 the characteristic length scale. Introducing the dimensionless quantities $\boldsymbol{u}_S = U_0\tilde{\boldsymbol{u}}_S$, $p_i = \Delta P_0 \tilde{p}_i$, $i = S, D$, and $\nabla(\cdot) = L_0^{-1}\tilde{\nabla}(\cdot)$ we arrive at the rescaled Stokes–Darcy system

$$\begin{aligned} \tilde{\nabla}\cdot\left(\mathrm{Re}^{-1}\mathrm{Eu}^{-1}\tilde{\boldsymbol{\epsilon}}(\tilde{\boldsymbol{u}}_S) + \tilde{p}_S\boldsymbol{I}\right) &= 0 \quad \text{in} \quad \tilde{\Omega}_S, \\ \tilde{\nabla}\cdot(\tilde{\boldsymbol{u}}_S) &= 0 \quad \text{in} \quad \tilde{\Omega}_S, \\ \tilde{\nabla}\cdot(-\mathrm{ReEuDa}\tilde{\nabla}\tilde{p}_D) &= 0 \quad \text{in} \quad \tilde{\Omega}_D, \end{aligned} \tag{4.3}$$

with the coupling conditions on Γ,

$$\begin{aligned} \boldsymbol{\tau}\cdot\tilde{\boldsymbol{\epsilon}}(\tilde{\boldsymbol{u}}_S)\cdot\boldsymbol{n} + \alpha\mathrm{Da}^{-1/2}\boldsymbol{\tau}\cdot\tilde{\boldsymbol{u}}_S &= \boldsymbol{0}, \\ \boldsymbol{n}\cdot\left(\mathrm{Re}^{-1}\mathrm{Eu}^{-1}\tilde{\boldsymbol{\epsilon}}(\tilde{\boldsymbol{u}}_S) + \tilde{p}_S\boldsymbol{I}\right)\cdot\boldsymbol{n} + \tilde{p}_D &= 0, \\ \tilde{\boldsymbol{u}}_S\cdot\boldsymbol{n} + \mathrm{ReEuDa}\tilde{\nabla}\tilde{p}_D\cdot\boldsymbol{n} &= 0. \end{aligned} \tag{4.4}$$

Here we introduced the dimensionless velocity gradient $\tilde{\boldsymbol{\epsilon}}(\tilde{\boldsymbol{u}}_S) = \tilde{\nabla}\tilde{\boldsymbol{u}}_S + \tilde{\nabla}^T\tilde{\boldsymbol{u}}_S$, the dimensionless numbers $\mathrm{Re} := \rho U_0 L_0 \mu^{-1}$, $\mathrm{Eu} := \Delta P_0 \rho_0^{-1} U_0^{-2}$, $\mathrm{Da} := kL_0^{-2}$, and ρ_0 denotes a characteristic fluid density. We recognize that our equation system is effectively characterized by a characteristic free-flow number $S = \mathrm{Re}^{-1}\mathrm{Eu}^{-1} = U_0 \mu L_0^{-1} \Delta P_0^{-1}$, the Darcy number, Da, and the Beavers–Joseph slip coefficient, α. Moreover, by comparing (4.3)–(4.4) with (2.1)–(2.4) we observe that for unit scaling parameters U_0, ΔP_0, ρ_0, and L_0 (as is the case in the manufactured problem (A.1)) we can interpret S, respectively, Da, as μ and k. To estimate the relevant ranges, we consider three examples.

Example 4.1 (channel flow over a regular porous medium in a micromodel). In [70], water flow in a micromodel with a free-flow channel of height 200 μm adjacent to a regular porous medium is examined at low Reynolds numbers, $U_0 \approx 0.2 - 0.4\ \mathrm{mm\,s^{-1}}$, $\mu = 10^{-3}$ Pa s. The slip coefficient α is determined as 2.26. The permeability can be estimated by Poiseuille flow in a bundle of tubes due to the regular geometry and is in the order of $k \approx 10^{-12} - 10^{-8}$ m^2. Hence, $S \approx 1$, $\mathrm{Da} \in [4 \cdot 10^{-4}, 4 \cdot 10^{0}]$, $\alpha = 2.26$.

Example 4.2 (air channel flow over porous medium box in a wind tunnel). Such a scenario may be modeled by the Stokes–Darcy system if the Reynolds number is sufficiently small ($\mathrm{Re} < 1$). Assuming a channel width of 0.1 m, air viscosity $\mu = 10^{-5}$ Pa s, and $\mathrm{Re} = 1$ yields $U_0 = 10^{-4}\ \mathrm{m\,s^{-1}}$. Such a velocity would only require $\Delta P_0 \approx 10^{-9}$ Pa (estimated assuming Poiseuille flow in a tube). Using a laboratory sand with $k \approx 10^{-12}$ m^2 yields $S \approx 10$, $\mathrm{Da} \approx 10^{-10}$, $\alpha \in [1, 10]$.

Example 4.3 (cerebrospinal fluid flow in subarachnoid space and brain cortex). The brain cortex can be considered a porous medium with $k \approx 10^{-18} - 10^{-16}$ m^2 [41]. The brain is surrounded by the subarachnoid space (SAS), a shallow void layer ($L_0 \approx 2$ mm) filled with a water-like fluid ($\mu = 10^{-3}$ Pa s). Typical Stokes velocities in SAS range between 10^{-3} and 1 $\mathrm{cm\,s^{-1}}$, and typical pressure gradients are on the order of 1 Pa, which gives $S \in [5 \cdot 10^{-4}, 5 \cdot 10^{-1}]$, $\mathrm{Da} \in [2.5 \cdot 10^{-13}, 2.5 \cdot 10^{-11}]$, $\alpha \in [1, 10]$.

4.3. Robustness study. Examples 4.1 to 4.3 reveal that $S \in [10^{-5}, 10^{1}]$, $\mathrm{Da} \in [10^{-14}, 10^{0}]$, $\alpha \in [0, 10^{2}]$ cover a wide range of relevant applications. Following the problem and solver setup described in Example 2.1, we report iterations of the preconditioned MinRes solver using the three Stokes–Darcy formulations (2.5), (2.8), and (2.10) with the numerically exact (LU-inverted) preconditioners (3.16), (3.19), and (3.24). Discretization in terms of both FEM and FVM is considered. We recall that due to the experimental setup, in particular, the unit sized scaling parameters (cf. (A.1)), the ranges identified in section 4.2 are effectively the ranges for μ, k, and α.

4.3.1. Preconditioning $\mathcal{A}^{\mathbf{Tr}}$. Using discretization by FEM, we investigate formulation (2.5) with preconditioner (3.16). Both conforming $\boldsymbol{P}_2$-P_1-P_2 and nonconforming $\boldsymbol{CR}_1$-P_0-P_0 elements are used. For the latter, we employ a facet stabilization [18] (see also (SM1.1)). We refer to Appendix A for approximation properties of these schemes for the Stokes–Darcy problem.

Starting with the conforming $\boldsymbol{P}_2$-P_1-P_2 elements, Figure 1 summarizes performance of (3.16) for the Trace formulation. Specifically, in each subplot corresponding to a fixed value of μ (varies in row), we plot the iteration count for different refinement levels, six different values of k indicated by color, and four different values of the slip coefficient α. It can be seen that the iterations are bounded in mesh size as well as the material parameters. Specifically, between 24 and 53 iterations are required for convergence in all cases. Furthermore, the (bounded) condition numbers of the preconditioned systems are reported in section SM2.

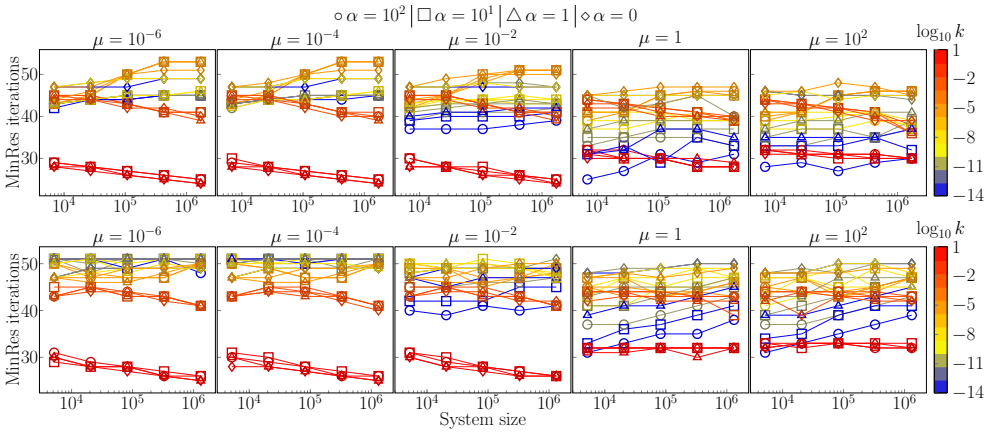

FIG. 1. *Performance of preconditioner* (3.16) *for the trace formulation* (2.5) *and the model problem from Example* 2.1 *with parameter ranges identified in section* 4.2. *Discretization by* $\boldsymbol{P}_2$-P_1-P_2 *elements (top) and* $\boldsymbol{CR}_1$-P_0-P_0 *elements (bottom) using stabilization* [18] *(see also* (SM1.1)*).*

For nonconforming $\boldsymbol{CR}_1$-P_0-P_0 elements, the results are given in the bottom panel of Figure 1. We observe that the iterations appear bounded, varying between 25 and 51. However, there is a modest increase[2] with h for $k = 10^{-14}$ and $\mu \geq 1$. We attribute this growth to round-off errors when inverting the preconditioner since the pressure block is then scaled with 10^{-16}-10^{-14}.

4.3.2. Preconditioning $\mathcal{A}^{\mathrm{La}}$ and $\mathcal{A}^{\mathrm{Ro}}$. We discuss robustness of (3.19) and (3.24) for the multiplier formulation (2.8) and the Robin formulation (2.10). Linear solver (MinRes) iterations over a large range of parameters are shown in Figure 2 and confirm parameter-robustness in both cases, with iteration counts between 10 and 39 for (3.19)-preconditioned $\mathcal{A}^{\mathrm{La}}$ and iteration counts between 1 and 48 for (3.24)–preconditioned $\mathcal{A}^{\mathrm{Ro}}$. We note that in particular when the ratio $\kappa = \mu^{-1}k$ is small, the reported iteration counts are very small (even one in the most extreme case) but stable for varying system sizes. We can attribute this to the specific configuration of the test case. With $\kappa \ll 1$ the contribution $\beta_n T_n' T_n$ in operator (3.20) dominates the Stokes block. We recall that $\beta_n := \kappa^{-1} h_K$. However, the right-hand side of the linear system only scales with μ for our particular case and both normal velocity and normal velocity gradient are zero in the exact solution (A.1)–(A.2). In this setting, the linear solver manages to reduce the very large initial defect (due to the combination of random initial guess in the range $[0, 1)$, large operator norm, and small right-hand side) by the requested factor of 10^8 in only one iteration. We remark that in this case the approximation of the solution is rather poor and a stricter convergence criterion would be required to obtain an accurate solution. However, this does not diminish the observation that the iterations are bounded. In consistency with all other results, we therefore report the results for the specified reduction of 10^8. This particularity does not affect the multiplier formulation since the term $\beta_n T_n' T_n$ is not present in operator (3.17). To fully convince the reader, we additionally report condition numbers of the discrete preconditioned operators in section SM3. The results show that the condition number stays between 5 and 17 for all reported parameter combinations. We note

[2]Between the smallest and the largest system considered the iterations grow by 10 while the system size increases by 3 orders of magnitude.

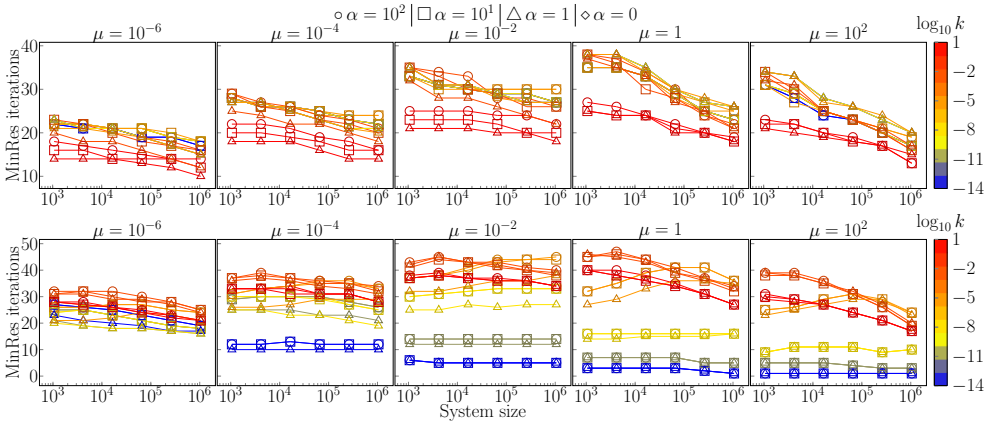

FIG. 2. *Iteration counts for the* (3.19)*-preconditioned multiplier formulation* (2.8) *(top) and* (3.24)*-preconditioned Robin formulation* (2.10) *(bottom). Discretization with FVM as described in section* SM1.

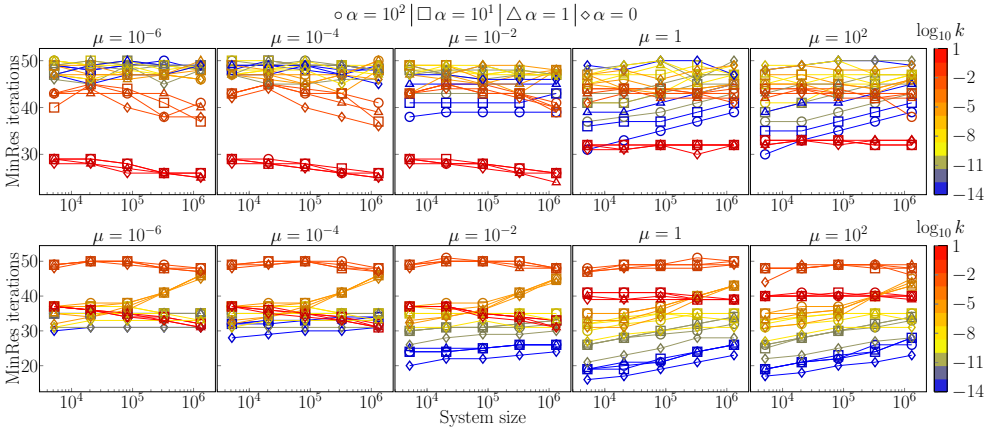

FIG. 3. *Iteration counts for the* (3.19)*-preconditioned Lagrange multiplier formulation* (2.8) *(top) and Robin formulation* (2.10) *with preconditioner* (3.24) *(bottom). Discretization by* $\boldsymbol{CR}_1$*-*P_0*-*P_0*(-*P_0*) elements.*

that the condition number estimates involving $\mathcal{B}^{\mathrm{Ro}}$ are reported over a smaller range of mesh sizes than in Figure 2 since the computations require an expensive assembly of an inverse of sum of two inverted matrices.

Preconditioners $\mathcal{B}^{\mathrm{La}}$ and $\mathcal{B}^{\mathrm{Ro}}$ were also investigated using nonconforming $\boldsymbol{CR}_1$-P_0-P_0(-P_0) elements. Results collected in Figure 3 confirm robustness of both preconditioners. The number of iterations remained between 24 and 50 for (3.19)-preconditioned $\mathcal{A}^{\mathrm{La}}$ and between 16 and 50 for $\mathcal{A}^{\mathrm{Ro}}$ with preconditioner (3.24).

4.4. Three-dimensional examples. The robustness study of section 4.3 concerned a two-dimensional setup leading to a relatively small interface with only a few hundred cells in Γ_h. Moreover, the preconditioners $\mathcal{B}^{\mathrm{Tr}}$, $\mathcal{B}^{\mathrm{La}}$, and $\mathcal{B}^{\mathrm{Ro}}$ were always computed exactly. To address the efficiency of the preconditioners in more practical scenarios, we next apply the proposed Stokes–Darcy solvers to two three-dimensional model problems. In particular, we investigate the effect of approximating

the action of the preconditioner blocks in terms of off-the-shelf multilevel methods. In addition, the problems are chosen such that we go beyond the assumptions on the interface (not a closed surface) and the boundary conditions (interface intersects with Neumann boundary) introduced at the end of section 2 to simplify the theoretical analysis.

In the following two examples, we investigate solvers for two of the proposed Stokes–Darcy formulations: (A) the Trace formulation (2.5) with preconditioner (3.16) and FEM discretization and (B) the Lagrange multiplier formulation (2.8) with preconditioner (3.19) discretized by FVM. We remind the reader that the FEM and FVM implementations differ in the software stack. In particular, all FEM results using direct solvers are obtained with MUMPS [2], while FVM results use UMFPACK [25]. The FEM results rely on Hypre's BoomerAMG [32], while for FVM the algebraic multigrid of dune-istl [12] is used. Moreover, the results are computed with different hardware setups: (A) Ubuntu workstation with AMD Ryzen Threadripper 3970X 32-Core processor and 128GB of memory, (B) openSUSE workstation with AMD Ryzen Threadripper 3990X 64-Core processor and 270GB of memory. However, in both cases the computations are run in serial restricted to one CPU.[3] Finally (and going more beyond the presented theory), the Stokes block in the FVM operators (3.17) and (3.19) is not symmetric due to a nonsymmetric stencil in the current implementation of boundary condition (2.3a) for the case of reentrant corners in the Stokes domain. However, the asymmetry is localized to the few dofs associated with the interface. As symmetry is a strict requirement for MinRes, we present GMRes iterations instead.

To evaluate efficiency of the proposed preconditioners, we compare their numerically exact realization to approximations in terms of multilevel methods. For (A) and BoomerAMG, the different approximations correspond to computing the action of each block by increasing numbers (same for each block for simplicity) of $\mathrm{V}(2,2)$ AMG cycles per application of the preconditioner. We used default settings except for the aggregation threshold which is set to 0.7, the recommended value for $3d$ problems. For (B) and Dune::AMG, the number of smoother iterations n on each level of a $\mathrm{V}(n,n)$-cycle was varied.

In addition, we compare the solvers, with the analogues of the naïve preconditioner presented in Example 2.1, that is, $\mathcal{B}^{\mathrm{Tr}}$, respectively, $\mathcal{B}^{\mathrm{La}}$, with the fractional operator omitted. (Moreover, in this case the pressure block of the preconditioner reads $-\kappa(\Delta + I)$ to avoid the singularity due to the Neumann boundary conditions on $\partial\Omega_D \setminus \Gamma$.)

4.4.1. Channel flow over porous hill. As the first model problem, we consider viscous flow over a porous medium with a curved interface; see Figure 4. Let $\alpha = 1$, $\mu = 10^{-3}$, and $k \in \{10^{-2}, 10^{-5}\}$. The fluid motion is driven by a pressure difference between the inlet and outlet where the (nonstandard) boundary conditions $p_S = \tilde{p}_S$ (inlet, $p_S = 0$ on the outlet) and $\boldsymbol{\tau} \cdot \boldsymbol{u}_S = \mathbf{0}$ (see, e.g., [37]) are prescribed.

On the rest of the fluid domain, we enforce $\boldsymbol{u}_S = \mathbf{0}$, while the boundary of the porous domain is impermeable (homogeneous Neumann boundary conditions). Therefore, newly, the interface intersects (mixed boundaries) $\Gamma_S^{\boldsymbol{u}}$ and Γ_D^u. The fact that Γ is incident to the Dirichlet boundary on the Stokes side translates to a modification of the preconditioner such that the fractional operator is now constructed with Dirichlet boundary conditions; see section SM2 for further details.

[3] Single threaded execution of all solver components is enforced by setting `OPM_NUM_THREADS=1`.

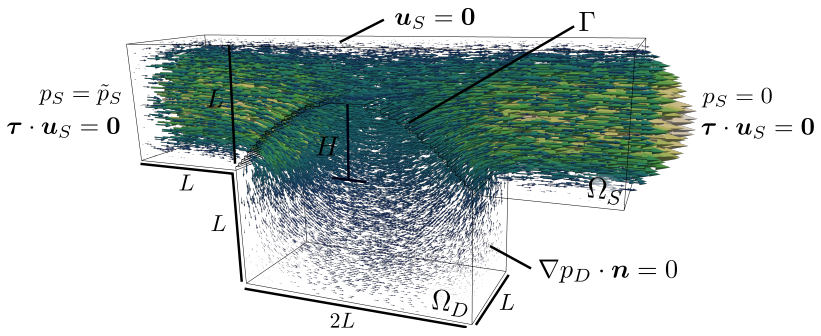

FIG. 4. *Setup for channel flow example in section* 4.4. *All boundaries are no-flow boundaries except for the right and left sides of the channel where we prescribe pressure and zero tangential velocities with* $\tilde{p}_S = 10^{-8}$. *The dimensions are given by* $L = 0.5$, $H = 0.3$ *and the interface* Γ *is chosen as a section of a cylinder with radius* $R = H/2 + L^2/(2H)$. *Arrows visualize the resulting velocity field for* $\mu = 10^{-3}$, $k = 10^{-2}$, $\alpha = 1$, *where longer, lighter arrows correspond to higher velocities.*

TABLE 2

Exact and approximate preconditioners for Stokes–Darcy problem in Figure 4 *using the Trace formulation* (2.5) *and preconditioner* (3.16). *Discretization by* $\boldsymbol{P}_2$-P_1-P_2. *MinRes iterations until convergence (reducing preconditioned residual norm by factor* 10^8*) with the preconditioner computed exactly (bLU) and by* $j\,V(2,2)$ *cycles of AMG are shown. The numbers in parentheses represent aggregate solver setup and solver runtime rounded to full seconds. (Top)* $k = 10^{-2}$. *(Bottom)* $k = 10^{-5}$. *In addition timings for solving* $\mathcal{A}^{Tr}$ *using a* direct *solver and preconditioned MinRes solver with the exact* naïve*-preconditioner of Example* 2.1 *are listed.*

dofs	$\lvert V_h\rvert$	bLU	1V(2,2)	2V(2,2)	4V(2,2)	Direct[a]	Naïve
3562	107	84 (1)	92 (1)	85 (1)	84 (1)	- (1)	98 (1)
13452	293	89 (2)	103 (2)	91 (3)	89 (5)	- (1)	106 (2)
69554	1023	88 (11)	112 (20)	92 (30)	88 (54)	- (4)	106 (9)
468646	3671	88 (173)	129 (265)	101 (388)	89 (646)	- (98)	108 (138)
3562	107	88 (1)	108 (1)	98 (1)	95 (1)	- (1)	1065 (2)
13452	293	92 (2)	123 (2)	106 (4)	101 (6)	- (1)	1538 (14)
69554	1023	93 (11)	143 (23)	110 (33)	98 (55)	- (4)	1659 (110)
468646	3671	97 (180)	164 (314)	122 (439)	105 (716)	- (98)	1661 (1293)

[a] MUMPS

Performance of the $\mathcal{B}^{\mathrm{Tr}}$-preconditioned formulation (2.5) discretized with the $\boldsymbol{P}_2$-P_1-P_2 FEM is summarized in Table 2. It can be seen that exact preconditioners lead to iterations bounded in refinement with little sensitivity to the change in permeability. In addition, the LU-based preconditioners are noticeably faster[4] than the AMG-based approximation. We remark that with LU at most 30% of the reported time was spent in the setup phase which was dominated by factorization of the blocks. To give an example of the cost of the eigensolver, for the finest interface mesh reported in Table 4, $|V_h| = 13976$, assembly of the fractional block takes 256 s. However, the presence of the resulting (large) dense block in the matrix of the pressure preconditioner also affects factorization time and the cost per Krylov iteration.

For preconditioners realized by AMG cycles robustness in h requires at least four V cycles if $k = 10^{-2}$ while eight cycles are needed for $k = 10^{-5}$. This result supports our observation (not reported here) that black-box algebraic multigrid is not a parameter-robust preconditioner for the pressure block in (3.16). Specifically, AMG

[4]Due to the used (mostly default) settings the timings of AMG should be considered a pessimistic bound for the performance.

TABLE 3

Exact and approximate preconditioners for Stokes–Darcy problem in Figure 4 using formulation (2.8) and preconditioner $\mathcal{B}^{La}$ (3.19). Discretization with FVM (Staggered-TPFA). GMRes iterations (reducing preconditioned residual norm by factor 10^8) are shown. In parentheses, we provide wall clock times (aggregate solver setup and runtime) rounded to full seconds. Table shows results for $k = 10^{-2}$ (top), $k = 10^{-5}$ (middle), $k = 10^{-12}$ (bottom). In addition timings for solving $\mathcal{A}^{La}$ using a direct *solver and preconditioned GMRes solver with the exact* naïve*-preconditioner constructed by omission of the fractional component in $\mathcal{B}^{La}$ are included.*

dofs	$\lvert V_h\rvert$	bLU	1V(1,1)	1V(2,2)	1V(4,4)	Direct[a]	Naïve
8640	208	60 (1)	83 (1)	71 (1)	64 (1)	- (1)	89 (1)
66342	832	64 (11)	109 (7)	92 (7)	81 (7)	- (6)	86 (13)
517552	3264	66 (337)	156 (132)	128 (134)	109 (146)	- (468)	84 (374)
8640	208	69 (1)	111 (1)	96 (1)	89 (1)	- (1)	330 (3)
66342	832	82 (13)	145 (8)	127 (8)	112 (9)	- (6)	403 (53)
517552	3264	91 (411)	201 (161)	169 (163)	147 (180)	- (485)	449 (1431)
8640	208	69 (1)	113 (1)	97 (1)	89 (1)	- (1)	4411 (158)
66342	832	83 (14)	147 (11)	130 (11)	116 (13)	- (6)	n/c[b]
517552	3264	99 (437)	203 (235)	180 (256)	161 (312)	- (533)	n/c[b]

[a] UMFPACK [b] not converged in under $10,000$ iterations

struggles when the interface term dominates the Laplacian in Ω_D. Finally, in agreement with Example 2.1 for $k = 10^{-5}$, the naïve preconditioner leads to considerably more iterations (and slower runtime) than $\mathcal{B}^{\mathrm{Tr}}$. However, none of the iterative approaches outperform the direct solver for the reported system sizes.

Performance of the $\mathcal{B}^{\mathrm{La}}$-preconditioned formulation (2.8) discretized with the Staggered-TPFA FVM is summarized in Table 3. In comparison with the FEM results but in consistency with observations in $2d$ examples in section 4.3, the solvers based on FVM and exact preconditioner initially show a slight increase of the number of iterations with refinement (in particular for small k). However, we point out that the difference in the number of iterations between consecutive grid refinements gets smaller and smaller (similar to what can be seen for the condition numbers in section SM3). While the solver with exact $\mathcal{B}^{\mathrm{La}}$ appears parameter-robust, it is evident that the naïve preconditioner (missing the fractional component) is not robust in k. When approximating all blocks with AMG, the fastest execution times could be achieved. In comparison with BoomerAMG, Dune::AMG uses a faster but less accurate interpolation strategy, which leads to considerably faster execution time per iteration. Increasing the number of smoother iterations reduces iteration counts but due to the increased cost per iteration does not result in a better performance. Moreover, the Dune::AMG-based solver does not show robustness with grid refinement, even for a large number of smoother iterations (we tested up to 64). However, the Dune::AMG-based solver appears robust in the model parameters.

4.4.2. Embedded porous blocks. In the second and final example, we consider viscous channel flow past and through two porous inclusions with different permeabilities; see Figure 5. From the point of view of assumptions of section 2, the novel feature is the fact that the interface is now formed by two closed surfaces.

Iterations counts and runtime estimates for various solvers are shown in Table 4 (FEM) and Table 5 (FVM). In general, the conclusions from section 4.4.1 apply to the new example as well. In particular, exact preconditioners $\mathcal{B}^{\mathrm{Tr}}$, $\mathcal{B}^{\mathrm{Tr}}$ yield iteration counts that are stable in mesh size.

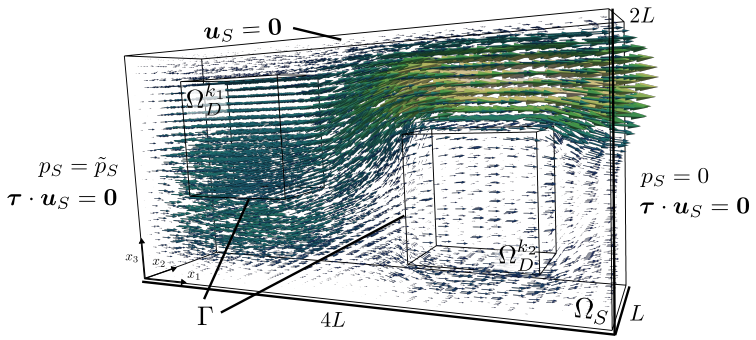

FIG. 5. *Setup for porous blocks example in section* 4.4. *All boundaries are no-flow boundaries except for the right and left sides of the channel where we prescribe pressure and zero tangential velocities with* $\tilde{p}_S = 10^{-8}$. *The channel dimension are given by* $L = 0.5$ *and the blocks are* $\Omega_D^{k_1} = [L/2, 3L/2] \times [2L/8, 7L/8] \times [3L/4, 7L/4]$ *and* $\Omega_D^{k_2} = [5L/2, 7L/2] \times [L/8, 6L/8] \times [1L/4, 5L/4]$ *and are assigned different permeabilities* $k_1 = 10^{-1}$, $k_2 = 10^{-3}$. *Moreover,* $\mu = 10^{-3}$, $\alpha = 1$. *The coarsest FVM discretization is a structured (anisotropic) rectangular cuboid mesh with* $16 \times 16 \times 16$ *cells. FEM results are computed with unstructured tetrahedral meshes.*

TABLE 4
Exact and approximate preconditioners for Stokes–Darcy problem in Figure 5 *using the Trace formulation* (2.5) *and preconditioner* (3.16). *Discretization by* $\boldsymbol{P}_2$-P_1-P_2. *Legend as in Table* 2.

dofs	$\lvert V_h \rvert$	bLU	1V(2,2)	2V(2,2)	4V(2,2)	Direct	Naïve
7256	484	123 (1)	143 (2)	129 (3)	125 (4)	- (1)	240 (2)
25260	1212	125 (4)	152 (8)	131 (13)	127 (21)	- (1)	257 (6)
124732	3768	125 (37)	162 (84)	133 (127)	126 (221)	- (12)	264 (46)
836293	13976	126 (932)	189 (1426)	144 (1909)	129 (3049)	- (370)	275 (721)

TABLE 5
Exact and approximate preconditioners for Stokes–Darcy problem in Figure 5 *using the Lagrange multiplier formulation* (2.8) *and preconditioner* (3.19). *Discretization by FVM. Legend as in Table* 3.

dofs	$\lvert V_h \rvert$	bLU	1V(1,1)	1V(4,4)	Direct	Naïve
16144	608	107 (4)	151 (3)	118 (3)	- (1)	257 (6)
122432	2432	109 (85)	192 (62)	147 (70)	- (64)	258 (138)
952576	9728	109 (3861)	281 (3458)	195 (3310)	- (5617)	187 (4806.8)

4.5. Nondiagonal preconditioners. Stemming from the operator preconditioning framework, the Stokes–Darcy preconditioners $\mathcal{B}^{\mathrm{Tr}}$, $\mathcal{B}^{\mathrm{La}}$, $\mathcal{B}^{\mathrm{Ro}}$ investigated in the preceding sections are block-diagonal operators, which from the linear algebra point of view form the Schur complement/natural norm preconditioners [56, 58]. However, once the Schur complement approximation is available, more involved preconditioners can be formulated, which are known to lead to reduced number of Krylov iterations, e.g., nonsymmetric upper/lower diagonal preconditioners [45] (for the GMRes solver). To allow for a direct comparison with the previously used MinRes solver, we illustrate next the reduction in iterations with a symmetric positive-definite block-LDU preconditioner based on the full Schur complement factorization. Taking the trace formulation $\mathcal{A}^{\mathrm{Tr}}$ as an example, the proposed preconditioner reads

$$\mathcal{B}_F^{\mathrm{Tr}} := \mathcal{B}_U^{\mathrm{Tr}} \mathcal{B}^{\mathrm{Tr}} (\mathcal{B}_U^{\mathrm{Tr}})',$$

TABLE 6

Number of MinRes iterations with block-LDU preconditioners. (Left) FEM and trace ($\boldsymbol{P}_2$-P_1-P_2) formulation. (Right) FV and Lagrange multiplier formulation. MinRes iteration counts with diagonal preconditioners are shown in the brackets. In all cases numerically exact operators are considered. Setup of Example 2.1 *is used with BJS constant set to* 1.

	$\mathcal{B}_F^{\mathrm{Tr}}$ (FEM)			$\mathcal{B}_F^{\mathrm{La}}$ (FV)	
#dofs \ (μ, k)	(1, 1)	$(10^{-4}, 10^{-6})$	#dofs \ (μ, k)	(1, 1)	$(10^{-6}, 10^{-5})$
1780	19(41)	27(51)	1072	13(29)	11(22)
6884	19(41)	27(52)	4192	13(27)	11(22)
27076	19(40)	28(54)	16576	13(26)	10(21)
107396	18(40)	28(54)	65920	12(22)	10(21)

where

$$\mathcal{B}_U^{\mathrm{Tr}} := \begin{bmatrix} I & -A^{-1}\nabla & -A^{-1}T_n' \\ & I & \\ & & I \end{bmatrix}^{-1},$$

and $A = -\nabla \cdot (2\mu\boldsymbol{\epsilon}) + \beta_\tau T_\tau' T_\tau$ being the leading block of $\mathcal{A}^{\mathrm{Tr}}$. Preconditioners for the remaining formulations are defined analogously.

Using the setup of Example 2.1, a random initial vector, and the tolerance of 10^{-10} for the relative preconditioned residual norm, it can be seen in Table 6 that convergence of the MinRes solver with the block-LDU preconditioners is achieved in approximately half the number of iterations as when their diagonal counterparts are used. The factor 2 is consistent with observations/analysis in literature; see, e.g., [68, 33]. We remark that fewer iterations do not necessarily imply a better performing solver in terms of total runtime, although we did achieve a speed-up for the FV solver using $\mathcal{B}_F^{\mathrm{La}}$ after exploiting some code optimization potential.

5. Conclusions and outlook. Our work concerned monolithic preconditioning of symmetric formulations of the coupled Stokes-primal Darcy problem which were motivated by differences in handling the interface coupling that are natural to finite element and finite volume methods. Parameter robust preconditioners for each of the three formulations were constructed based on the well-posedness of the problems established within a unifying functional framework. The proposed preconditioners are based on norms in fractional Sobolev spaces. Using discretization in terms of both FEM and FVM our numerical results demonstrated the parameter-robustness in several examples partly going beyond the presented theory in terms of boundary conditions and interface configuration. However, efficiency of the proposed solvers is currently suboptimal due to the realization of the pressure preconditioner, in particular, the reliance on the spectral form of the fractional interface operators. To improve efficiency of the proposed preconditioners scalable techniques for the parameter-robust approximation of the components, in particular, the pressure block, will be addressed in future work.

Appendix A. Numerical tests and manufactured solution. For the numerical grid convergence tests and parameter-robustness tests, we work with the manufactured solution given in [66] for unit parameters $\mu = 1$, $k = 1$, $\alpha = 1$ as

$$\text{(A.1a)} \qquad \boldsymbol{u}_S = \begin{bmatrix} -\frac{1}{\pi}\exp(x_2)\sin(\pi x_1) \\ (\exp(x_2) - \exp(1))\cos(\pi x_1) \end{bmatrix} \qquad \text{in} \quad \Omega_S,$$

$$\text{(A.1b)} \qquad p_S = 2\exp(x_2)\cos(\pi x_1), \qquad \text{in} \quad \Omega_S,$$

$$\text{(A.1c)} \qquad p_D = (\exp(x_2) - x_2\exp(1))\cos(\pi x_1) \qquad \text{in} \quad \Omega_D,$$

where $\Omega_D = [0,1] \times [0,1]$, $\Omega_F = [0,1] \times [1,2]$. Moreover, for the formulation with Lagrange multiplier,

$$\text{(A.1d)} \qquad \lambda = p_D(x_1, x_2 = 1) = 0 \qquad \text{on} \quad \Gamma,$$

where $\Gamma = [0,1] \times \{1\}$. To obtain the same solution over the whole range of parameters, we use the source terms

$$\text{(A.2a)} \qquad \boldsymbol{f}_S := \begin{bmatrix} \frac{1}{\pi}\exp(x_2)\sin(\pi x_1)(\mu - \mu\pi^2 - 2\pi^2) \\ \cos(\pi x_1)(\mu\left((\pi^2+1)\exp(x_2) - \pi^2\exp(1)\right)) + 2(1-\mu)\exp(x_2)) \end{bmatrix},$$

$$\text{(A.2b)} \qquad f_D := \frac{k}{\mu}\cos(\pi x_1)\left((\pi^2+1)\exp(x_2) - \pi^2 x_2\exp(1)\right),$$

and modified coupling conditions

$$\text{(A.3a)} \qquad \boldsymbol{\tau}\cdot\boldsymbol{\sigma}(\boldsymbol{u}_S, p_S)\cdot\boldsymbol{n} + \beta_\tau \boldsymbol{\tau}\cdot\boldsymbol{u}_S = h_\tau^\Gamma, \quad h_\tau^\Gamma := (\beta_\tau - \mu)\frac{1}{\pi}\exp(x_2)\sin(\pi x_1),$$

$$\text{(A.3b)} \qquad \boldsymbol{n}\cdot\boldsymbol{\sigma}(\boldsymbol{u}_S, p_S)\cdot\boldsymbol{n} + p_D = h_n^\Gamma, \quad h_n^\Gamma := 2(\mu-1)\exp(1)\cos(\pi x_1),$$

$$\text{(A.3c)} \qquad \boldsymbol{u}_S\cdot\boldsymbol{n} + \kappa\nabla p_D\cdot\boldsymbol{n} = g^\Gamma, \quad g^\Gamma := 0.$$

The functions h_τ^Γ, h_n^Γ, and g^Γ ensure that the conditions are satisfied independent of the choice of parameters. Note that the choice of data in (A.3) only modifies the right-hand side while the problem operators remain unchanged.

This setting enables code verification in terms of grid convergence tests in all parameter settings. For grid convergence tests, the errors for the finite element schemes are reported in L^2 and H^1 norms. Using $\boldsymbol{P}_2$-P_1-P_2 elements for (2.5) quadratic convergence in all the variables in their respective norms is expected. Discretization by $\boldsymbol{CR}_1$-P_0-P_0(-P_0) in all the formulations yields a first-order scheme.

The errors for the finite volume scheme are computed in the following discrete L^2 norm:

$$\text{(A.4)} \qquad \|u\|_{\mathrm{FV}} := \left(\sum_{K\in\Omega_h} |K| u_K^2\right)^{\frac{1}{2}}.$$

It is well known that with the typical flux reconstruction schemes, based on a TPFA on structured Cartesian grids, second order superconvergence at cell centers (pressures) and face centers (Stokes velocity components) is obtained [51, 30, 64].

We report error convergence of the FEM schemes for all the formulations in Figure 6. Expected (or faster) convergence is observed in all cases. We remark that the observed quadratic convergence of the interfacial pressure $p|_\Gamma$ in (2.8) is likely due to the zero exact solution in the manufactured setup. Error convergence for the FVM schemes is reported for formulations (2.8) and (2.10) in Figure 7. Quadratic convergence in the discrete norm (A.4) is observed for all the variables.

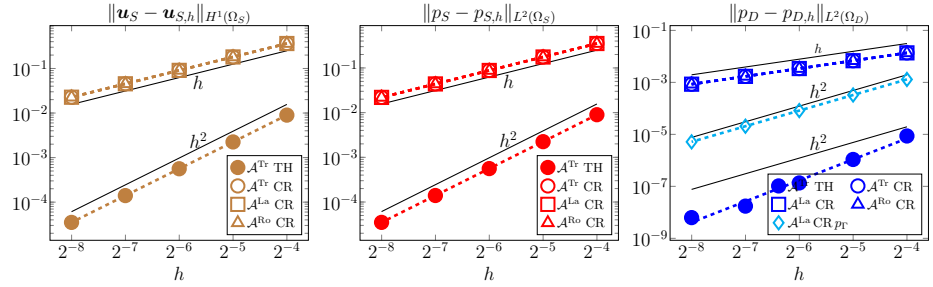

FIG. 6. *Approximation properties of FEM discretizations for the manufactured problem* (A.1) *with unit parameters using the Trace formulation* (2.5)*, multiplier formulation* (2.8)*, and Robin formulation* (2.10)*. Only* (2.5) *is considered with* $\boldsymbol{P}_2$*-*P_1*-*P_2*, while* $\boldsymbol{CR}_1$*-*P_0*-*P_0*(-*P_0*) is used for all formulations.* $L^2(\Gamma)$*-error of interface pressure in* (2.8) *is plotted in cyan.*

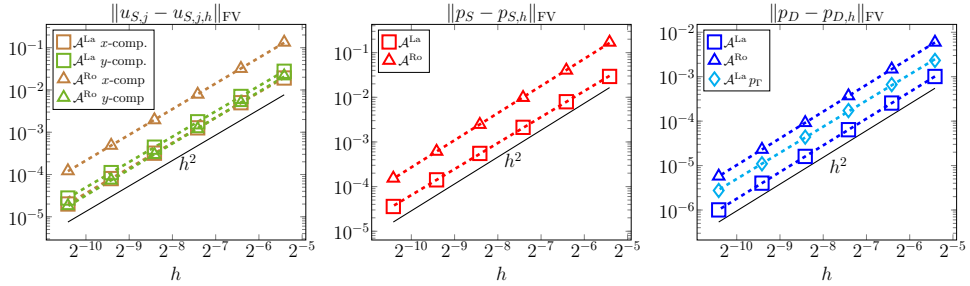

FIG. 7. *Approximation properties of FVM (Staggered-TPFA) discretization for the manufactured problem* (A.1) *with unit parameters using the Lagrange multiplier formulation* (2.8) *and the Robin formulation* (2.10)*.* $u_{S,x}$ *and* $u_{S,y}$ *denote the components of* $\boldsymbol{u}_S$ *(the dofs for the respective components have different locations and control volumes in the staggered FVM). For* (2.8) *the error of interface pressure error measured in* L^2*-norm* (A.4) *on* Γ *is plotted in cyan.*

REFERENCES

[1] S. Ackermann, C. Bringedal, and R. Helmig, *Multi-scale three-domain approach for coupling free flow and flow in porous media including droplet-related interface processes*, J. Comput. Phys., 429 (2021), 109993, https://doi.org/10.1016/j.jcp.2020.109993.

[2] P. Amestoy, I. S. Duff, J. Koster, and J.-Y. L'Excellent, *A fully asynchronous multifrontal solver using distributed dynamic scheduling*, SIAM J. Matrix Anal. Appl., 23 (2001), pp. 15–41.

[3] K. Baber, K. Mosthaf, B. Flemisch, R. Helmig, S. Muthing, and B. Wohlmuth, *Numerical scheme for coupling two-phase compositional porous-media flow and one-phase compositional free flow*, IMA J. Appl. Math., 77 (2012), pp. 887–909, https://doi.org/10.1093/imamat/hxs048.

[4] S. Badia and R. Codina, *Unified stabilized finite element formulations for the Stokes and the Darcy problems*, SIAM J. Numer. Anal., 47 (2009), pp. 1971–2000.

[5] T. Bærland, M. Kuchta, and K.-A. Mardal, *Multigrid methods for discrete fractional Sobolev spaces*, SIAM J. Sci. Comput., 41 (2019), pp. A948–A972.

[6] T. Bærland, M. Kuchta, K.-A. Mardal, and T. Thompson, *An observation on the uniform preconditioners for the mixed darcy problem*, Numer. Methods Partial Differential Equations, 36 (2020), pp. 1718–1734.

[7] S. Balay, S. Abhyankar, M. F. Adams, et al., *PETSc/TAO Users Manual*, Tech. report ANL-21/39 - Revision 3.16, Argonne National Laboratory, 2021.

[8] P. Bastian, M. Blatt, A. Dedner, C. Engwer, R. Klöfkorn, R. Kornhuber, M. Ohlberger, and O. Sander, *A generic grid interface for parallel and adaptive scientific computing. Part* II*: Implementation and tests in DUNE*, Computing, 82 (2008), pp. 121–138, https://doi.org/10.1007/s00607-008-0004-9.

[9] G. S. Beavers and D. D. Joseph, *Boundary conditions at a naturally permeable wall*, J. Fluid Mech., 30 (1967), pp. 197–207, https://doi.org/10.1017/s0022112067001375.

[10] J. Bergh and J. Löfström, *Interpolation Spaces: An Introduction*, Grundlehren Math. Wisse., Springer, Berlin, 2012.
[11] N. Birgle, R. Masson, and L. Trenty, *A domain decomposition method to couple non-isothermal compositional gas liquid Darcy and free gas flows*, J. Comput. Phys., 368 (2018), pp. 210–235, https://doi.org/10.1016/j.jcp.2018.04.035.
[12] M. Blatt, *A Parallel Algebraic Multigrid Method for Elliptic Problems with Highly Discontinuous Coefficients*, Ph.D. thesis, University of Heidelberg, Germany, 2010, https://doi.org/10.11588/HEIDOK.00010856.
[13] M. Blatt and P. Bastian, *The iterative solver template library*, in Applied Parallel Computing. State of the Art in Scientific Computing: 8th International Workshop, PARA 2006, Umeå, Sweden, Springer, Berlin, 2007, pp. 666–675, https://doi.org/10.1007/978-3-540-75755-9_82.
[14] W. M. Boon, *A parameter-robust iterative method for Stokes-Darcy problems retaining local mass conservation*, ESAIM Math. Model. Numer. Anal., 54 (2020), pp. 2045–2067.
[15] W. M. Boon, M. Kuchta, K.-A. Mardal, and R. Ruiz-Baier, *Robust preconditioners and stability analysis for perturbed saddle-point problems—application to conservative discretizations of Biot's equations utilizing total pressure*, SIAM J. Sci. Comput., 43 (2021), pp. B961–B983.
[16] D. Braess, *Stability of saddle point problems with penalty*, ESAIM Math. Model. Numer. Anal., 30 (1996), pp. 731–742.
[17] J. Bramble, J. Pasciak, and P. Vassilevski, *Computational scales of Sobolev norms with application to preconditioning*, Math. Comput., 69 (2000), pp. 463–480.
[18] E. Burman and P. Hansbo, *Stabilized Crouzeix-Raviart element for the Darcy-Stokes problem*, Numer. Methods Partial Differential Equations, 21 (2005), pp. 986–997, https://doi.org/https://doi.org/10.1002/num.20076.
[19] E. Burman and P. Hansbo, *A unified stabilized method for Stokes' and Darcy's equations*, J. Comput. Appl. Math., 198 (2007), pp. 35–51.
[20] M. Cai, M. Mu, and J. Xu, *Preconditioning techniques for a mixed Stokes/Darcy model in porous media applications*, J. Comput. Appl. Math., 233 (2009), pp. 346–355.
[21] A. Caiazzo, V. John, and U. Wilbrandt, *On classical iterative subdomain methods for the Stokes–Darcy problem*, Comput. Geosci., 18 (2014), pp. 711–728.
[22] W. Chen, M. Gunzburger, F. Hua, and X. Wang, *A parallel Robin–Robin domain decomposition method for the Stokes–Darcy system*, SIAM J. Numer. Anal., 49 (2011), pp. 1064–1084.
[23] P. Chidyagwai, S. Ladenheim, and D. B. Szyld, *Constraint preconditioning for the coupled Stokes–Darcy system*, SIAM J. Sci. Comput., 38 (2016), pp. A668–A690.
[24] E. Coltman, M. Lipp, A. Vescovini, and R. Helmig, *Obstacles, interfacial forms, and turbulence: A numerical analysis of soil–water evaporation across different interfaces*, Trans. Porous Media, 134 (2020), pp. 275–301, https://doi.org/10.1007/s11242-020-01445-6.
[25] T. A. Davis, *Algorithm 832: UMFPACK V4.3—an unsymmetric-pattern multifrontal method*, ACM Trans. Math. Software, 30 (2004), pp. 196–199, https://doi.org/10.1145/992200.992206.
[26] M. Discacciati and L. Gerardo-Giorda, *Optimized Schwarz methods for the Stokes–Darcy coupling*, IMA J. Numer. Anal., 38 (2018), pp. 1959–1983.
[27] M. Discacciati, E. Miglio, and A. Quarteroni, *Mathematical and numerical models for coupling surface and groundwater flows*, Appl. Numer. Math., 43 (2002), pp. 57–74.
[28] M. Discacciati and A. Quarteroni, *Navier-Stokes/Darcy coupling: modeling, analysis, and numerical approximation*, Rev. Mat. Complut, 22 (2009), pp. 315–426.
[29] M. Discacciati, A. Quarteroni, and A. Valli, *Robin–Robin domain decomposition methods for the Stokes–Darcy coupling*, SIAM J. Numer. Anal., 45 (2007), pp. 1246–1268.
[30] J. Droniou and N. Nataraj, *Improved L^2 estimate for gradient schemes and superconvergence of the TPFA finite volume scheme*, IMA J. Numer. Anal., 38 (2017), pp. 1254–1293, https://doi.org/10.1093/imanum/drx028.
[31] A. Ern and J.-L. Guermond, *Theory and Practice of Finite Elements*, Appl. Math. Sci. 159, Springer, New York, 2013.
[32] R. D. Falgout and U. M. Yang, *hypre: A library of high performance preconditioners*, in Computational Science — ICCS 2002, P. M. A. Sloot, A. G. Hoekstra, C. J. K. Tan, and J. J. Dongarra, eds., Springer, Berlin, 2002, pp. 632–641.
[33] B. Fischer, A. Ramage, D. J. Silvester, and A. J. Wathen, *Minimum residual methods for augmented systems*, BIT, 38 (1998), pp. 527–543.
[34] T. Führer, *Multilevel decompositions and norms for negative order Sobolev spaces*, Math. Comput., to appear.

[35] J. Galvis and M. Sarkis, *Non-matching mortar discretization analysis for the coupling Stokes-Darcy equations*, Electron. Trans. Numer. Anal, 26 (2007), 07.
[36] G. N. Gatica, S. Meddahi, and R. Oyarzúa, *A conforming mixed finite-element method for the coupling of fluid flow with porous media flow*, IMA J. Numer. Anal., 29 (2008), pp. 86–108.
[37] V. Girault, *Curl-conforming finite element methods for Navier-Stokes equations with non-standard boundary conditions in R^3*, in The Navier-Stokes Equations Theory and Numerical Methods, Springer, New York, 1990, pp. 201–218.
[38] V. Girault, D. Vassilev, and I. Yotov, *Mortar multiscale finite element methods for Stokes–Darcy flows*, Numer. Math., 127 (2014), pp. 93–165.
[39] G. Guennebaud, B. Jacob, et al., *Eigen v3*, http://eigen.tuxfamily.org, 2010.
[40] V. Hernandez, J. E. Roman, and V. Vidal, *SLEPc: A scalable and flexible toolkit for the solution of eigenvalue problems*, ACM Trans. Math. Software, 31 (2005), pp. 351–362.
[41] K. E. Holter, B. Kehlet, A. Devor, T. J. Sejnowski, et al., *Interstitial solute transport in 3d reconstructed neuropil occurs by diffusion rather than bulk flow*, Proc. Natl. Acad. Sci. USA, 114 (2017), pp. 9894–9899, https://doi.org/10.1073/pnas.1706942114.
[42] K. E. Holter, M. Kuchta, and K.-A. Mardal, *Robust Preconditioning of Monolithically Coupled Multiphysics Problems*, preprint, arXiv:2001.05527, 2020.
[43] Q. Hong, J. Kraus, M. Lymbery, and F. Philo, *A New Framework for the Stability Analysis of Perturbed Saddle-Point Problems and Applications in Poromechanics*, preprint, arXiv:2103.09357, 2021.
[44] T. Karper, K.-A. Mardal, and R. Winther, *Unified finite element discretizations of coupled Darcy–Stokes flow*, Numer. Methods Partial Differential Equations, 25 (2009), pp. 311–326.
[45] A. Klawonn, *Block-triangular preconditioners for saddle point problems with a penalty term*, SIAM J. Sci. Comput., 19 (1998), pp. 172–184.
[46] T. Koch, B. Flemisch, R. Helmig, R. Wiest, and D. Obrist, *A multiscale subvoxel perfusion model to estimate diffusive capillary wall conductivity in multiple sclerosis lesions from perfusion mri data*, Int. J. Numer. Methods Biomed. Eng., 36 (2020), e3298, https://doi.org/https://doi.org/10.1002/cnm.3298.
[47] T. Koch, D. Gläser, K. Weishaupt, et al., *DuMu^x 3 - an open-source simulator for solving flow and transport problems in porous media with a focus on model coupling*, Comput. Math. Appl., 81 (2021), pp. 423–443, https://doi.org/10.1016/j.camwa.2020.02.012.
[48] M. Kuchta, *Assembly of multiscale linear PDE operators*, in Numerical Mathematics and Advanced Applications, ENUMATH 2019, F. J. Vermolen and C. Vuik, eds., Springer, Cham, 2021, pp. 641–650.
[49] M. Kuchta, M. Nordaas, J. Verschaeve, M. Mortensen, and K.-A. Mardal, *Preconditioners for saddle point systems with trace constraints coupling 2D and 1D domains*, SIAM J. Sci. Comput., 38 (2016), pp. B962–B987.
[50] W. J. Layton, F. Schieweck, and I. Yotov, *Coupling fluid flow with porous media flow*, SIAM J. Numer. Anal., 40 (2002), pp. 2195–2218.
[51] J. Li and S. Sun, *The superconvergence phenomenon and proof of the MAC scheme for the Stokes equations on non-uniform rectangular meshes*, J. Sci. Comput., 65 (2014), pp. 341–362, https://doi.org/10.1007/s10915-014-9963-5.
[52] P. Luo, C. Rodrigo, F. J. Gaspar, and C. W. Oosterlee, *Uzawa smoother in multigrid for the coupled porous medium and Stokes flow system*, SIAM J. Sci. Comput., 39 (2017), pp. S633–S661.
[53] K.-A. Mardal and R. Winther, *Preconditioning discretizations of systems of partial differential equations*, Numer. Linear Algebra Appl., 18 (2011), pp. 1–40, https://doi.org/10.1002/nla.716.
[54] A. Mikelić and W. Jäger, *On the interface boundary condition of Beavers, Joseph, and Saffman*, SIAM J. Appl. Math., 60 (2000), pp. 1111–1127, https://doi.org/10.1137/s003613999833678x.
[55] K. Mosthaf, K. Baber, B. Flemisch, R. Helmig, A. Leijnse, I. Rybak, and B. Wohlmuth, *A coupling concept for two-phase compositional porous-medium and single-phase compositional free flow*, Water Resources Research, 47 (2011), https://doi.org/doi.org/10.1029/2011WR010685.
[56] M. Murphy, G. Golub, and A. Wathen, *A note on preconditioning for indefinite linear systems*, SIAM J. Sci. Comput., 21 (2000), pp. 1969–1972.
[57] P. Oswald, *Multilevel norms for $H^{-1/2}$*, Computing, 61 (2007), pp. 235–255.
[58] J. Pestana and A. J. Wathen, *Natural preconditioning and iterative methods for saddle point systems*, SIAM Rev., 57 (2015), pp. 71–91.

[59] Y. Qiu, *Spectra*. https://github.com/yixuan/spectra, 2019.
[60] B. Rivière, *Analysis of a discontinuous finite element method for the coupled Stokes and Darcy problems*, J. Sci. Comput., 22–23 (2005), pp. 479–500, https://doi.org/10.1007/s10915-004-4147-3.
[61] B. Rivière and I. Yotov, *Locally conservative coupling of Stokes and Darcy flows*, SIAM J. Numer. Anal., 42 (2005), pp. 1959–1977.
[62] E. Rohan, J. Turjanicová, and V. Lukeš, *Multiscale modelling and simulations of tissue perfusion using the Biot-Darcy-Brinkman model*, Comput. Structures, 251 (2021), 106404, https://doi.org/https://doi.org/10.1016/j.compstruc.2020.106404.
[63] P. G. Saffman, *On the boundary condition at the surface of a porous medium*, Stud. Appl. Math., 50 (1971), pp. 93–101, https://doi.org/10.1002/sapm197150293.
[64] M. Schneider, D. Gläser, B. Flemisch, and R. Helmig, *Comparison of finite-volume schemes for diffusion problems*, Oil & Gas Science and Technology, 73 (2018), 82, https://doi.org/10.2516/ogst/2018064.
[65] M. Schneider, K. Weishaupt, D. Gläser, W. M. Boon, and R. Helmig, *Coupling staggered-grid and MPFA finite volume methods for free flow/porous-medium flow problems*, J. Comput. Phys., 401 (2020), 109012, https://doi.org/10.1016/j.jcp.2019.109012.
[66] M.-C. Shiue, K. C. Ong, and M.-C. Lai, *Convergence of the MAC scheme for the Stokes/Darcy coupling problem*, J. Sci. Comput., 76 (2018), pp. 1216–1251, https://doi.org/10.1007/s10915-018-0660-7.
[67] J. H. Smith and J. A. Humphrey, *Interstitial transport and transvascular fluid exchange during infusion into brain and tumor tissue*, Microvascular Research, 73 (2007), pp. 58–73.
[68] B. S. Southworth and S. A. Olivier, *A Note on* 2×2 *Block-Diagonal Preconditioning*, preprint, arXiv:2001.00711, 2020.
[69] R. Stevenson and R. van Venetië, *Uniform preconditioners of linear complexity for problems of negative order*, Comput. Methods Appl. Math., 21 (2021), pp. 469–478, https://doi.org/doi:10.1515/cmam-2020-0052.
[70] A. Terzis, I. Zarikos, K. Weishaupt, G. Yang, X. Chu, R. Helmig, and B. Weigand, *Microscopic velocity field measurements inside a regular porous medium adjacent to a low reynolds number channel flow*, Phys. Fluids, 31 (2019), 042001, https://doi.org/10.1063/1.5092169.